Available online at www.sciencedirect.com
ScienceDirect
Chemical Physics Letters 446 (2007) 344–349
CHEMICAL PHYSICS LETTERS
www.elsevier.com/locate/cplett

Influence of segregated adsorption on mixture diffusion in DDR zeolite

R. Krishna *, J.M. van Baten

Van 't Hoff Institute for Molecular Sciences, University of Amsterdam, Nieuwe Achtergracht 166, 1018 WV Amsterdam, The Netherlands

Received 17 July 2007; in final form 17 August 2007
Available online 24 August 2007

Abstract

Grand Canonical Monte Carlo simulations for adsorption of CO_2/CH_4, CH_4/N_2, and CO_2/Ar mixtures in DDR zeolite show that the window regions contain practically no CH_4 or Ar; these molecules are predominantly adsorbed within the cages. CO_2 and N_2 molecules adsorb both within the cages and at the window regions. Due to segregated adsorption, the ideal adsorbed solution theory is unable to predict the mixture loadings accurately. Molecular dynamics simulations show that CO_2 molecules that are strongly adsorbed at the windows hinder the inter-cage diffusion of partner molecules in mixtures; this effect is not described by the Maxwell–Stefan theory.

1. Introduction

DDR zeolite membranes offer technological possibilities for separation of CO_2/CH_4 and CH_4/N_2 mixtures [1–4]. In the design and development of zeolite membrane based separation technologies, the ideal adsorbed solution theory (IAST) of Myers and Prausnitz [5] is widely used to calculate the adsorption loadings of mixtures of molecules using only pure component isotherm fits as data inputs [6]. A key assumption of the IAST is that the composition of the adsorbed phase is spatially uniform within the zeolite; this assumption is not always a good one. Segregation effects, i.e. preferential location of molecules at certain sites or regions, have been observed for a variety of guest-host combinations in zeolites [7–13]. For adsorption of hydrocarbon mixtures in MFI, for example, branched and cyclic hydrocarbons are preferentially located at the intersections of the straight and zig-zag channels, whereas linear molecules can locate anywhere in the pores [14–16]. Murthi and Snurr [16] and Krishna and Paschek [10] have shown that such segregation effects for adsorption causes departures from ideality of adsorbed phase equilibria. The first objective of the present communication is to show that segregation effects are present for CO_2/CH_4, CH_4/N_2, and CO_2/Ar mixture adsorption in DDR. We show that segregation effects cause the failure of IAST to provide a good *quantitative* representation of component loadings. The second major objective is to demonstrate that segregation effects also influence mixture diffusion. We show that the Maxwell–Stefan (M–S) diffusion equations, commonly used to predict mixture diffusion on the basis of information on pure component diffusivity data, fails in the presence of segregation effects.

Grand Canonical Monte Carlo (GCMC) simulations were carried out to determine pure component and mixture isotherms, and probability distribution of molecules in cages and windows. Molecular dynamics (MD) simulations were performed to determine self-diffusivities for mixture diffusion in DDR. The simulation methodologies are detailed in the Supplementary Material accompanying this publication.

2. Segregation effects in adsorption

DDR consists of cages separated by narrow elliptical shape windows of 3.6–4.4 Å size. For adsorption of

* Corresponding author. Fax: +31 20 5255604.
E-mail address: r.krishna@uva.nl (R. Krishna).

0009-2614/$ - see front matter © 2007 Elsevier B.V. All rights reserved.
doi:10.1016/j.cplett.2007.08.060

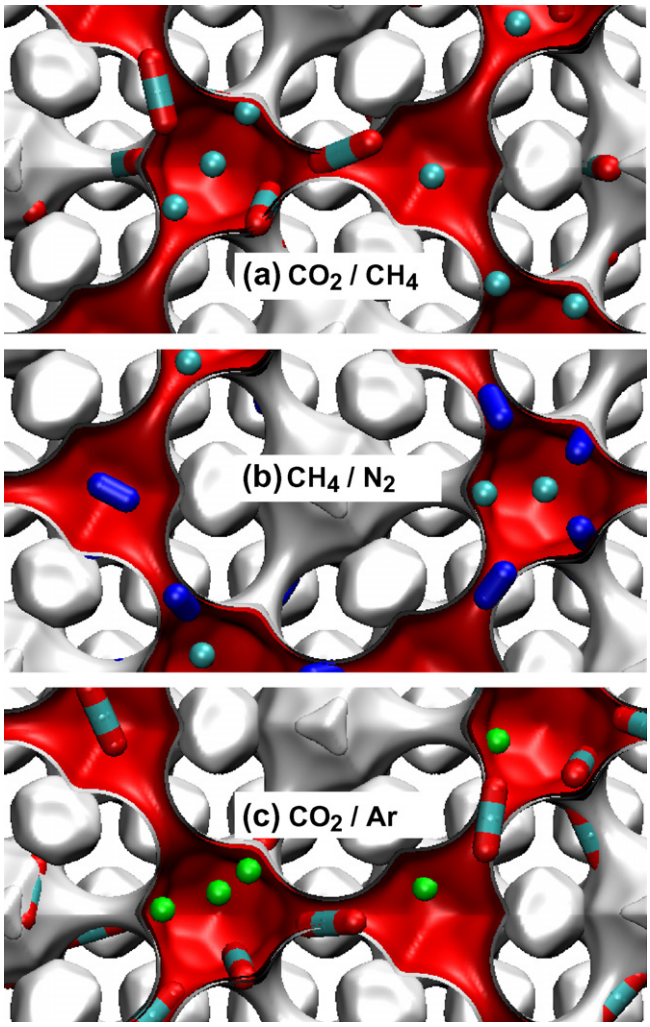

Fig. 1. Snapshots obtained from NVT simulations of mixtures in DDR at 300 K. The molecular loadings are taken to be equal for either component in the mixture.

CO_2/CH_4, CH_4/N_2, and CO_2/Ar mixtures, CO_2 and N_2 molecules can locate inside the cages and also at the windows, straddling two cages; see as the NVT snaps in Fig. 1. Due to their somewhat larger diameters CH_4 and Ar feel too constrained at the windows and prefer to locate within the cages. In order to quantify the segregation effects we carried out GCMC simulations for the three mixtures at partial fugacities $f_1 = f_2 = 1$ MPa and 300 K. For 10^7 equilibration cycles the centers of the molecules were captured every 1000 cycles, starting at cycle 1000. The window region is considered to be a sphere with a diameter of 3 Å. If the centre of the molecule falls within the spheres it is taken as belong to the window region. The remainder of the molecules is taken as belong to the cage region. By summing over the all the 10^4 samples, reliable statistics were obtained for the % probability of adsorbing a molecule within the window region; see Table 1. The collected statistics also yields ratios of the loadings of CO_2/CH_4, CH_4/N_2, and CO_2/Ar at the window region, and in the entire pore structure of DDR.

Table 1
Probability distribution of locating molecules in window region, and within cages for equimolar binary mixtures in DDR at partial fugacities of 1 MPa and 300 K

System	Component	Location at window region (%)	Ratio of molecules within cages	Ratio of molecules in total pore structure
CO_2/CH_4	CO_2	43	2.9	5
	CH_4	0.2		
CH_4/N_2	CH_4	0.5	6.6	5.9
	N_2	10		
CO_2/Ar	CO_2	37	18.8	29.3
	Ar	2.4		

For the CO_2/CH_4 mixture, we note the ratio of the number of adsorbed molecules of CO_2 to that of CH_4 within the entire DDR pore space equals 5, whereas within the cages this ratio is 2.9. Segregation effects reduce the competition within the cages faced by CH_4 from CO_2. The GCMC simulations are compared with the IAST predictions in Fig. 2a. We note that the IAST significantly under-predicts the loading of the more weakly adsorbed CH_4. These results are in agreement with the findings of Chen and Sholl [17]. The conventional IAST calculation assumes that CH_4 molecules compete with *all* of the CO_2, making no allowance for segregation. The IAST anticipates a stiffer competition between CO_2 and CH_4 as it assumes a uniform distribution of composition; consequently the separation selectivity is *over* estimated. We also note that the predictions of the IAST become progressively worse with increasing gas phase fugacities. For the CO_2/Ar mixture the CO_2/Ar ratio within the entire DDR pore space is 29.3, whereas within the cages this ratio is 18.8; Ar faces a less stiff competition within the cages from CO_2 than anticipated by the IAST and therefore the IAST underpredicts the Ar loading; see Fig. 2b.

For CH_4/N_2 mixture adsorption, the situation is somewhat different. There is a 10% probability of locating N_2 at the window region. At the window regions N_2 faces no suppressing competition from CH_4 molecules. The IAST predictions for N_2 are lower than the GCMC simulations; see Fig. 2c.

The extent of non-ideality of adsorption can be quantified by backing out the activity coefficients of the individual species. This requires an appropriate definition of the standard states and compliance with the Gibbs–Duhem constraint; see Murthi and Snurr [16] and Chen and Sholl [17] for details.

3. Segregation effects on mixture diffusion

MD simulation results of pure component self-diffusivities, $D_{i,\text{self}}$, and M–S diffusivities, $Đ_i$, of CO_2, CH_4, N_2, Ar, Ne, He, H_2, and O_2 in DDR are presented in Fig. 3a,b. The diffusivities vary by about five orders of magnitude and the hierarchy is dictated by the degree of confinement of the

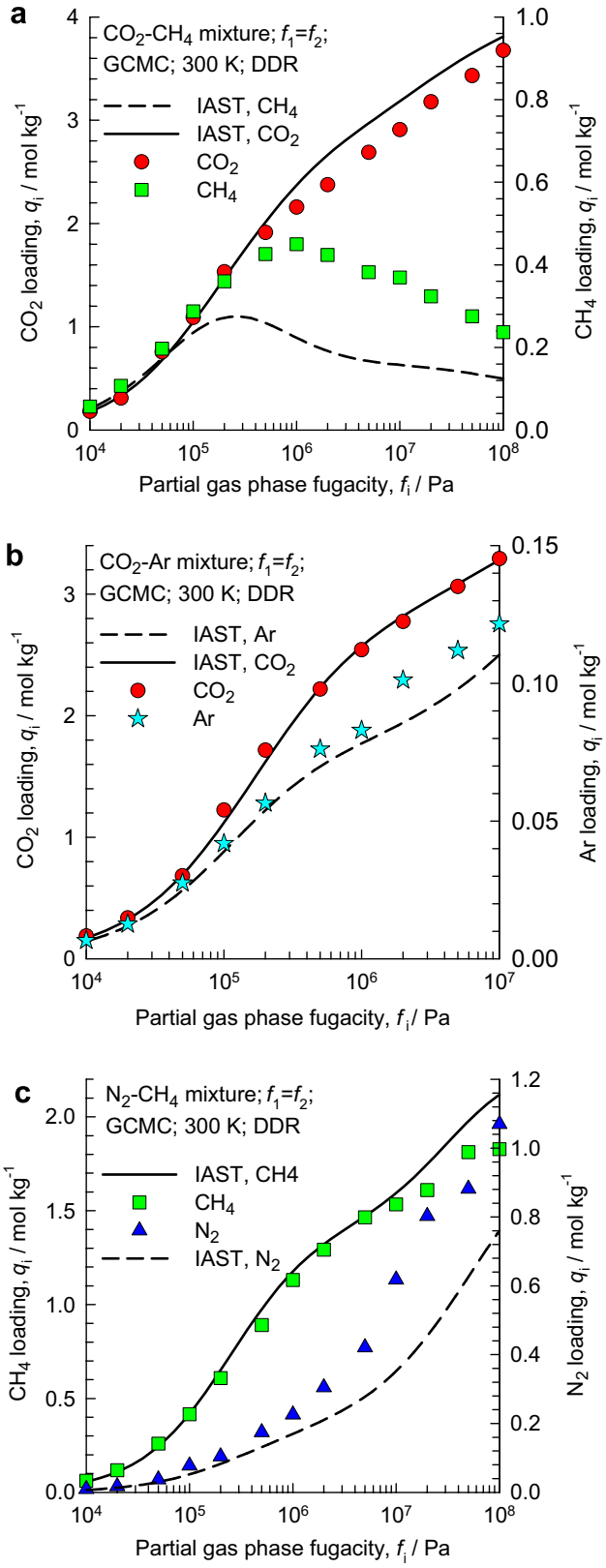

Fig. 2. GCMC simulations of the component loadings in (a) CO_2/CH_4, (b) CO_2/Ar, and (c) CH_4/N_2, gas mixtures in DDR at 300 K compared with the calculations of IAST, shown by the continuous solid lines. For all mixtures the partial gas phase fugacities are equal, i.e. $f_1 = f_2$.

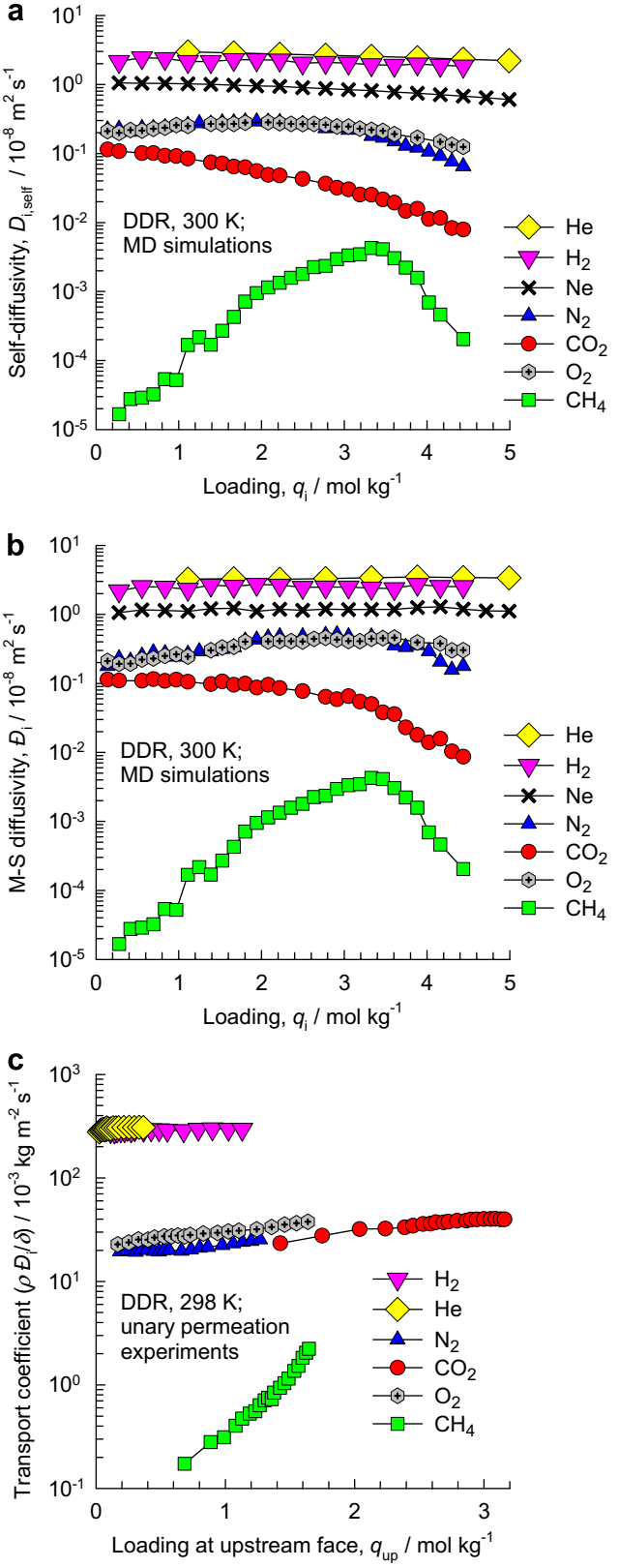

Fig. 3. MD simulations of (a) self-diffusivities, $D_{i,\mathrm{self}}$, and (b) M–S diffusivities $Đ_i$ of CO_2, CH_4, N_2, Ne, He, H_2, and O_2 in DDR at 300 K. (c) Transport coefficients, $\rho Đ_i/\delta$, of CO_2, CH_4, N_2, He, H_2, and O_2 across a DDR membrane at 298 K backed out from data of Himeno et al. [3].

Table 2
Self-exchange parameters a_i and b_i defined by Eq. (2) for various molecules in DDR zeolite

Component	a_i	b_i	Saturation capacity, $q_{i,\text{sat}}$/mol kg^{-1}
Ne	1	2.5	14
Ar	4	3	5.4
CO_2	1.6	1.7	4.6
N_2	3.2	4	5.4
CH_4	5	0	4.2

molecules at the windows of DDR [18]. Strongly confined CH_4 exhibits a strong increase in diffusivity with loading, reaches a maximum and then decreases as the loading approaches saturation. Generally speaking, for self-diffusion in binary mixtures each species will influence the mobility of the other. The $D_{i,\text{self}}$ of the more mobile species will be reduced, and the $D_{i,\text{self}}$ of the tardier species will be increased. The mutual influence of the component species are due to correlation effects [18]. In the M–S theory correlation effects are quantified by self-exchange ($\mathbb{D}_{ii}$) and binary exchange ($\mathbb{D}_{ij}$) coefficients. The self-diffusivities in the mixture can be calculated from pure component $\mathbb{D}_i$ using [18,19]:

$$D_{1,\text{self}} = 1\Big/\left(\frac{1}{\mathbb{D}_1}+\frac{q_1}{q_{1,\text{sat}}\mathbb{D}_{11}}+\frac{q_2}{q_{2,\text{sat}}\mathbb{D}_{12}}\right);$$
$$D_{2,\text{self}} = 1\Big/\left(\frac{1}{\mathbb{D}_2}+\frac{q_2}{q_{2,\text{sat}}\mathbb{D}_{22}}+\frac{q_1}{q_{1,\text{sat}}\mathbb{D}_{21}}\right) \quad (1)$$

The self-exchange coefficients $\mathbb{D}_{ii}$ are determined from self- and M–S diffusivities of pure components and correlated in the form [18]:

$$\frac{\mathbb{D}_{ii}}{\mathbb{D}_i} = a_i \exp\left(-b_i\frac{q_i}{q_{i,\text{sat}}}\right) \quad (2)$$

The values of a_i, b_i, and $q_{i,\text{sat}}$ for CO_2, N_2, Ne, Ar, and CH_4 are summarized in Table 2. For CH_4 correlation effects are negligibly small and $\frac{\mathbb{D}_{ii}}{\mathbb{D}_i}$ is estimated to be 5. The binary exchange coefficients $\mathbb{D}_{12}$ and $\mathbb{D}_{21}$ are calculated using

$$q_{2,\text{sat}}\mathbb{D}_{12} = [q_{2,\text{sat}}\mathbb{D}_{11}]^{q_1/(q_1+q_2)}[q_{1,\text{sat}}\mathbb{D}_{22}]^{q_2/(q_1+q_2)} = q_{1,\text{sat}}\mathbb{D}_{21} \quad (3)$$

The preferential adsorption of CO_2 at the windows of DDR can be expected to have an *additional* hindering influence on the inter-cage hopping of partner molecules such CH_4, Ar, N_2, or Ne in the mixture. MD simulations of the $D_{i,\text{self}}$ in CO_2/Ar mixture for a total mixture loading, $q = q_1 + q_2 = 2.77$ mol/kg, are shown in Fig. 4a. Here, Ar is the more mobile species and there is a slight speeding-up of tardier CO_2 with increasing presence of Ar; this is as expected. With increasing proportion of CO_2 the diffusivity of Ar is significantly reduced; when the mole fraction of CO_2 in the mixture exceeds 0.7, Ar is found to have a lower diffusivity than CO_2.

The calculations of the M–S theory following Eq. (1) are shown by the continuous solid lines in Fig. 4a. We note that while the predictions for CO_2 are in reasonable agreement with the MD simulations, the M–S theory fails to anticipate the severe reduction in the Ar diffusivity with increased CO_2 loading. The hindrance effect due to adsorbed CO_2 in the window regions experienced by Ar manifests in the *mixture*, and this effect cannot be predicted on the basis of only *pure component* diffusivity data. The reason for this failure is that the M–S theory only caters for correlation effects that cause slowing down of the more mobile species; the M–S formulation does not cater for the *additional* hindrance effect due to CO_2.

CO_2 exercises a similar hindrance effect in CO_2/Ne and CO_2/N_2 mixtures; see Fig. 4b and c. Again the M–S theory significantly underestimates the reduction in the $D_{i,\text{self}}$ of the more mobile species Ne and N_2.

Fig. 4d shows MD simulation data for CO_2/CH_4 mixtures. With increasing concentration of the tardier CH_4, the $D_{i,\text{self}}$ of more mobile CO_2 decreases, as is to be expected. Indeed, the M–S model anticipates this decrease. More remarkably the $D_{i,\text{self}}$ of the tardier CH_4 is further reduced with increasing proportion of CO_2; this influence is attributable to the hindrance experienced by CH_4 to hop between cages due to the presence of strongly adsorbed CO_2 in the window regions; see animations of our MD simulations[20]. The M–S model is not capable of anticipating a decrease in the CH_4 diffusivity.

For CH_4/N_2 mixture, the diffusivity of the tardier CH_4 decreases even more in the presence of N_2 molecules, some of which are lodged at the windows; see Fig. 4e.

When neither component in the mixture is significantly adsorbed at the window region, we should not expect the hindrance effects discussed above. This is indeed found to be the case for CH_4/Ar mixtures; see Fig. 4f; Eq. (1) is reasonably successful in the predicting the $D_{i,\text{self}}$ in this mixture.

4. Experimental data of Himeno et al. [3]

Himeno et al.[3] have published experimental data on unary permeation of CO_2, CH_4, N_2, He, H_2, and O_2 across a DDR membrane at 298 K. From their experimental data we backed out transport coefficients $\rho\mathbb{D}_i/\delta$; Fig. 3c presents $\rho\mathbb{D}_i/\delta$ as a function of the total mixture loading at the upstream face. The hierarchy of diffusivities is in good agreement with those determined from MD simulations. The loading dependence of $\rho\mathbb{D}_i/\delta$ for any molecule is also in broad agreement with the MD simulation results; compare Fig. 3b and c. Of particular note is the strong increase in the $\mathbb{D}_i$ of CH_4 in the range of loadings 0–3 mol/kg observed both in experiments and in the MD simulations. From the CO_2/CH_4 mixture permeation data of Himeno et al. [3], the backed out *effective* transport coefficients $\rho\mathbb{D}_i/\delta$ are presented in Fig. 5. We note that $\rho\mathbb{D}_i/\delta$ of either species is lower in the mixture than for pure components, in line with the MD simulation results presented in Fig. 4d. There is a slight slowing down of the more mobile CO_2

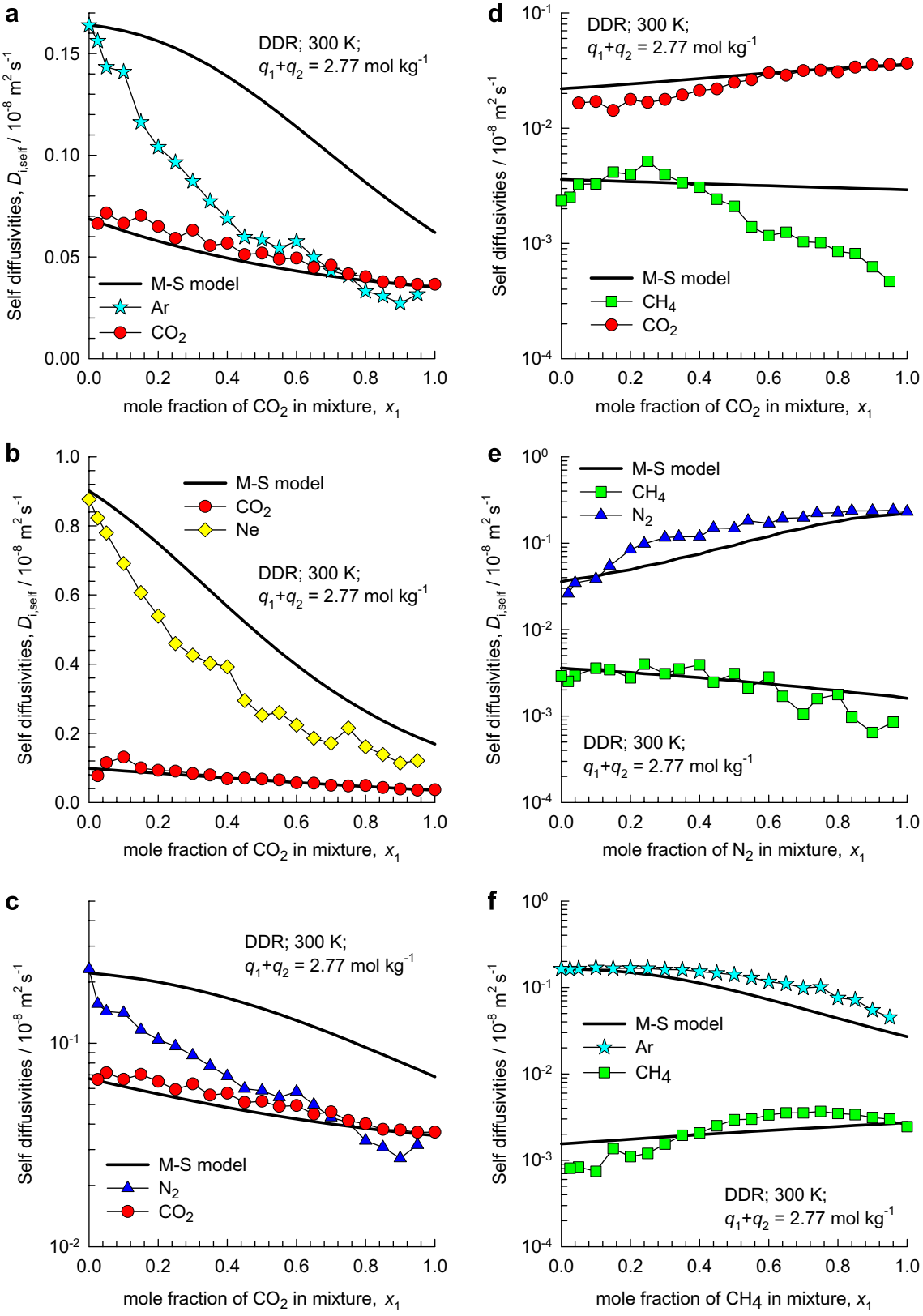

Fig. 4. Self-diffusivities in (a) CO_2/Ar, (b) CO_2/Ne, (c) CO_2/N_2, (d) CO_2/CH_4, (e) CH_4/N_2, and (f) CH_4/Ar mixtures in DDR at 300 K obtained at a total mixture loading of 2.77 mol/kg. The continuous solid lines are calculations using Eq. (1).

due to the tardy CH_4. More interestingly, we note that for CH_4 the diffusivity in the mixture is about an order of magnitude lower than the unary permeation value; this reduction is most likely due to the hindrance effect of strongly

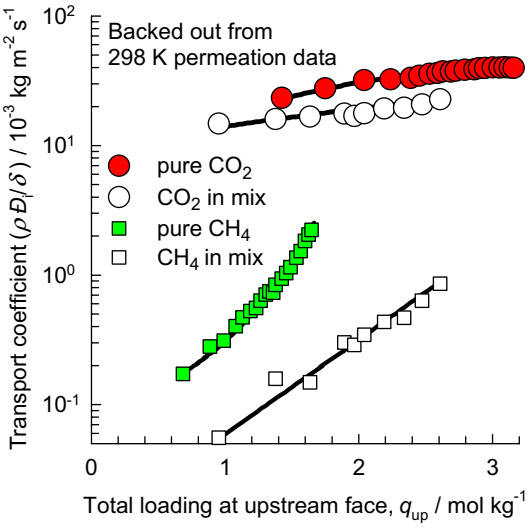

Fig. 5. Comparison of transport coefficients, $\rho Đ_i/\delta$, for DDR membrane backed out from unary and binary mixture permeation of CO_2/CH_4 reported by Himeno et al. [3].

adsorbed CO_2 at the window regions. Segregation effects enhance the CO_2/CH_4 diffusion selectivity.

5. Conclusions

GCMC simulations reveal the segregated nature of adsorption of CO_2/CH_4, CH_4/N_2, and CO_2/Ar mixtures in DDR. CO_2 and N_2 molecules locate both within the cages and at the windows, whereas CH_4 and Ar adsorb predominantly within the cages. The IAST does not adequately describe the component loadings for mixture adsorption and there are strong non-ideality effects especially for CO_2/CH_4 mixtures. Another important consequence of segregation is that the adsorbed CO_2 and N_2 molecules at the window regions hinder the inter-cage transport of partner molecules such as CH_4, Ar, N_2, or Ne. Such hindrance effect is not catered for by the Maxwell–Stefan diffusion theory.

There is a need to develop improved models for mixture adsorption and diffusion that takes account of the segregation effects described in this Letter; work is in progress to develop such models.

Appendix A. Supplementary data

Supplementary data associated with this article can be found, in the online version, at doi:10.1016/j.cplett.2007.08.060.

References

[1] T. Tomita, K. Nakayama, H. Sakai, Micropor. Mesopor. Mat. 68 (2004) 71.
[2] R. Krishna, J.M. Van Baten, Chem. Eng. J. 133 (2007) 121.
[3] S. Himeno, T. Komatsu, S. Fujita, T. Tomita, K. Suzuki, K. Nakayama, S. Yoshida, Kagaku Kogaku Ronbun. 33 (2007) 122.
[4] J. van den Bergh et al., Stud. Surf. Sci. Catal. 170 (2007) 1021.
[5] A.L. Myers, J.M. Prausnitz, A. I. Ch. E. J. 11 (1965) 121.
[6] R. Krishna, J.M. van Baten, E. García-Pérez, S. Calero, Ind. Eng. Chem. Res. 46 (2007) 2974.
[7] L.A. Clark, A. Gupta, R.Q. Snurr, J. Phys. Chem. B 102 (1998) 6720.
[8] R. Krishna, B. Smit, S. Calero, Chem. Soc. Rev. 31 (2002) 185.
[9] J.M. van Baten, R. Krishna, Micropor. Mesopor. Mat. 84 (2005) 179.
[10] R. Krishna, D. Paschek, Phys. Chem. Chem. Phys. 3 (2001) 453.
[11] M. Schenk, S.L. Vidal, T.J.H. Vlugt, B. Smit, R. Krishna, Langmuir 17 (2001) 1558.
[12] A. Gupta, L.A. Clark, R.Q. Snurr, Langmuir 16 (2000) 3910.
[13] A. Gupta, R.Q. Snurr, J. Phys. Chem. B 109 (2005) 1822.
[14] R. Krishna, B. Smit, T.J.H. Vlugt, J. Phys. Chem. A 102 (1998) 7727.
[15] T.J.H. Vlugt, R. Krishna, B. Smit, J. Phys. Chem. B 103 (1999) 1102.
[16] M. Murthi, R.Q. Snurr, Langmuir 20 (2004) 2489.
[17] H. Chen, D.S. Sholl, Langmuir 23 (2007) 6431.
[18] R. Krishna, J.M. van Baten, Micropor. Mesopor. Mat. (2007), doi:10.1016/j.micromeso.2007.04.036.
[19] R. Krishna, J.M. van Baten, J. Phys. Chem. B 109 (2005) 6386.
[20] J.M. van Baten, R. Krishna, MD animations of diffusion in zeolites, University of Amsterdam, http://www.science.uva.nl/research/cr/animateMD/, 15 July 2007.

Supplementary Material to accompany:

Influence of segregated adsorption on mixture diffusion in DDR zeolite

R. Krishna*, J.M. van Baten

Van 't Hoff Institute for Molecular Sciences, University of Amsterdam, Nieuwe Achtergracht 166,

1018 WV Amsterdam, The Netherlands

1. GCMC simulation methodology

The adsorption isotherms for CO_2, CH_4, N_2, Ar, Ne, He, H_2, and O_2 in DDR were computed using Monte Carlo (MC) simulations in the grand canonical (GC) ensemble. The crystallographic data are available elsewhere.[1] The zeolite lattices are rigid during simulations, with static atomic charges that are assigned by choosing q_{Si} = +2.05 and q_O = -1.025, following the works of Jaramillo and Auerbach [2] and Calero et al.[3]. CH_4 molecules are described with a united atom model, in which each molecule is treated as a single interaction center.[4] CO_2 molecules are taken linear and rigid, with bond length C-O of 1.16Å and partial charges distributed around each molecule to reproduce experimental quadrupole moment. The interaction between adsorbed molecules is described with Coulombic and Lennard-Jones terms. The Coulombic interactions in the system are calculated by Ewald summation for periodic systems[5]. The parameters for CH_4 are taken from Dubbeldam et al[6] and Calero et al.[3]. CO_2 molecules are taken linear and rigid with bond length C–O of 1.16Å according to the 3LJ3CB.EPM2 model developed by Harris and Young [7]. We use the 2LJ3CB.MSKM model for N_2 dumbbell molecules with a rigid interatomic bond of 1.098Å[8, 9]. The partial charges of N_2 and CO_2 are distributed around each molecule to reproduce experimental quadrupole moment. The interactions between adsorbed molecules and the zeolite are dominated by dispersive forces between the pseudo-atoms and the oxygen atoms of the zeolite [10, 11] and the interactions of silicon and aluminium are considered through an effective potential with only the oxygen atoms. The Lennard-Jones parameters for CH_4-zeolite interactions are taken from Dubbeldam et al.[6]. The Lennard-Jones parameters for CO_2-zeolite and N_2-zeolite interactions are essentially those of Makrodimitris et al.[9]. The force field for He, Ne and Ar is taken from the paper by Skoulidas and Sholl[12]. The force field for H_2 corresponds to that given by Kumar et al.[13] In implementing this force field, quantum effects for H_2 have been ignored because the work of Kumar et al.[13] has shown that quantum effects are of negligible importance for temperatures above 200 K; all our simulations were performed at 300 K. The force field of Kumar et al.[13] is quite similar to that used by Gallo et al. [14]. The force field for O_2 is

taken from the work of Mellot and Lignieres[15]. Table 1 summarizes the information on the force fields for all gases.

The Lennard-Jones potentials are shifted and cut at 12 Å. The number of unit cells in the simulation box was chosen such that the minimum length in each of the coordinate directions was larger than 24 Å. Periodic boundary conditions were employed. Further GCMC simulation details are available in earlier publications[3, 6, 16].

The GCMC simulations were performed using the BIGMAC code developed by T.J.H. Vlugt[17] as basis. The code was modified to handle rigid molecular structures and charges. S. Calero is gratefully acknowledged for her technical inputs in this regard. Detailed validation of the force fields used for CH_4, CO_2, and N_2 is available elsewhere[6, 18].

Comparisons between experimental data and GCMC simulations for CH_4, CO_2, N_2, and O_2 in DDR are given in Figures 1, 2, 3, and 4. These data give an indication of the validity of the force fields.

2. MD simulation methodology

Diffusion is simulated using Newton's equations of motion until the system properties, on average, no longer change in time. The Verlet algorithm is used for time integration. A time step of 1 fs was used in all simulations. For each simulation, *initializing* GCMC moves are used to place the molecules in the domain, minimizing the energy. Next, follows an *equilibration* stage. These are essentially the same as the production cycles, only the statistics are not yet taken into account. This removes any initial large disturbances in the system do not affect statistics. After a fixed number of initialization and equilibrium steps, the MD simulation *production* cycles start. For every cycle, the statistics for determining the mean square displacements (MSDs) are updated. The MSDs are determined for time intervals ranging from 2 fs to 1 ns. In order to do this, an order-*N* algorithm, as detailed in Chapter 4 of Frenkel and Smit[5] is implemented. The Nosé-Hoover thermostat is applied to all the diffusing particles.

The DLPOLY code[19] was used along with the force field implementation as described in the previous section. DL_POLY is a molecular dynamics simulation package written by W. Smith, T.R.

Forester and I.T. Todorov and has been obtained from CCLRCs Daresbury Laboratory via the website.[19]

The MD simulations were carried out on clusters of PCs equipped with Intel Xeon processors running at 3.4 GHz on the Linux operating system. Each MD simulation, for a specified loading, was run for 120 h, determined to be long enough to obtain reliable statistics for determination of the diffusivities.

The self-diffusivities, $D_{\mathrm{i,self}}$, were computed by analyzing the mean square displacement of each species i for each of the coordinate directions:

$$D_{i,self} = \frac{1}{2n_i} \lim_{\Delta t \to \infty} \frac{1}{\Delta t} \left\langle \left(\sum_{l=1}^{n_i} \left(\mathbf{r}_{l,i}(t + \Delta t) - \mathbf{r}_{l,i}(t) \right)^2 \right) \right\rangle \tag{1}$$

In this expression n_{i} represents the number of molecules of species i respectively, and $\mathbf{r}_{\mathrm{l,i}}(t)$ is the position of molecule l of species i at any time t. The expression (1) also defines the self-diffusivity in a n-component mixture. For DDR the reported diffusivities are the averages in x- and y- directions $D = \left(D_x + D_y \right) / 2$.

For single component diffusion, the Maxwell-Stefan diffusivity was determined for each of the coordinate directions from

$$Đ_i = \frac{1}{2} \lim_{\Delta t \to \infty} \frac{1}{N_i} \frac{1}{\Delta t} \left\langle \left(\sum_{l=1}^{N_i} \left(\mathbf{r}_{l,i}(t + \Delta t) - \mathbf{r}_{l,i}(t) \right) \right)^2 \right\rangle \tag{2}$$

The self-exchange coefficient $Đ_{\mathrm{ii}}$ were calculated from

$$Đ_{ii} = \frac{\theta_i}{\dfrac{1}{D_{i,self}} - \dfrac{1}{Đ_i}} \tag{3}$$

where θ_{i} is the fractional occupancy:

$$\theta_i = \frac{q_i}{q_{i,sat}} \tag{4}$$

The values of the saturation capacities $q_{i,sat}$ were determined from GCMC simulations of the isotherms.

3. Pure component isotherms and fits

The GCMC simulated data for pure component isotherms for CO_2, CH_4, N_2, Ar, Ne, He, H_2, and O_2 in DDR at 300 K are presented in Figures 5. The GCMC simulation results, shown by the filled symbols in Figure 5, are in good agreement with the experimental data (open symbols) of Himeno et al. [20, 21], indicated by the open symbols in Figure 5. The continuous solid lines in Figure 5 are 3-site Langmuir fits of the isotherms

$$q = \frac{q_{sat,A} b_A f}{1 + b_A f} + \frac{q_{sat,B} b_B f}{1 + b_B f} + \frac{q_{sat,C} b_C f}{1 + b_C f} \qquad (5)$$

It was found impossible to fit any of the component isotherms with either a 2-site or single site Langmuir model. The 3-site Langmuir fits are "empirical" and the individual sites cannot be identified with specific locations within DDR. In eq. (5) q is the molar loading expressed in mol kg^{-1}, $q_{sat,A}$ is the saturation loading of site A, and f is the fugacity of the bulk gas phase. The values of the fitted parameters b and q_{sat} are specified in Table 2.

4. Probability density plots and segregation data for DDR

DDR consists of cages separated by narrow elliptical shaped windows of 3.6 – 4.4 Å size; for the purposes of quantifying segregation effects we have defined the window region to be a sphere with a diameter of 3 Å, as indicated by the blue spheres in Figure 6.

The GCMC simulations were run for 10^7 cycles. The centers of the molecules were captured every 1000 cycles (starting at cycle 1000). Each cycle performs a number of trial moves that is determined by MAX(20, number of molecules). For low pressures this means 20 moves per cycle, for higher pressures this means the number of trial moves per cycle equals the number of molecules. If the centre of the

molecule falls within the blue spheres it is taken as belong to the window region. The total number of molecules within the simulation box was also determined. The percentage of molecules in the windows was calculated by determining the percentage of molecule centers that were within a distance of 1.5 Å from a window center with respect to the total number of captured molecule centers. The remainder of the molecules is taken as belong to the cage region.

For adsorption of CO_2/CH_4, CH_4/N_2, and CO_2/Ar mixtures with partial fugacities $f_1 = f_2 = 1$ MPa and 300 K, the probability density snapshots in Figures 7, 8, and 9 indicate that segregation effects are present in the mixtures; no CH_4 or Ar molecules are visible in the window regions.

5. GCMC mixture simulations

For adsorption of CO_2/CH_4, CH_4/N_2, and CO_2/Ar mixtures, the GCMC mixture simulations of the component loadings are compared with the predictions of Ideal Adsorbed Solution Theory (IAST) of Myers and Prausnitz[22] in Figures 10, 11, and 12. For the IAST predictions, the pure component isotherm 3-site Langmuir fits given in Table 2 were used.

6. Analysis of Himeno data for CO_2/CH_4 permeation across DDR membrane

Himeno et al.[23] have published experimental data on unary permeation of CO_2, CH_4, N_2, He, H_2, and O_2 across a DDR membrane at 298 K. Their flux data has been replotted in Figure 13. We analysed their flux vs upstream pressure data and backed out the effective transport coefficients using the pure component isotherm fits of the GCMC simulated isotherms (cf. Table 2). The values of the transport coefficients $\rho Đ / \delta$ were backed out from each experimental point using

$$N = \frac{\rho Đ}{\delta} DF \tag{6}$$

Where DF, the driving force for unary permeation is [24]

$$DF = q_{sat,A} \ln\left(\frac{1 + b_A f_{up}}{1 + b_A f_{down}}\right) + q_{sat,B} \ln\left(\frac{1 + b_B f_{up}}{1 + b_B f_{down}}\right) + q_{sat,C} \ln\left(\frac{1 + b_C f_{up}}{1 + b_C f_{down}}\right) \tag{7}$$

The 3-site Langmuir constants are as given in Table 2. In backing out the transport coefficients, we assumed a value of the downstream pressure = 50 kPa. Figure 14 presents the backed out data on the transport coefficients of CO_2, CH_4, N_2, He, H_2, and O_2 as a function of the loading at the upstream face of the membrane, q_{up}.

Himeno et al.[23] have also presented data for permeation fluxes across a DDR membrane for CO_2/CH_4 mixtures with equal fugacities in the bulk gas phase on the upstream side of the membrane; Figure 15. The effective transport coefficients of each of the two components in the binary mixture was determined from the individual fluxes using

$$\frac{\rho Đ_i}{\delta} = \frac{N_i}{\int\limits_{upstream}^{downstream} \sum\limits_{j=1}^{2} \left(\Gamma_{ij} \frac{dq_j}{dx} \right) dx}; \quad i = 1,2 \tag{8}$$

The thermodynamic factors Γ_{ij} are defined as

$$\frac{q_i}{RT} \frac{d\mu_i}{dx} = \sum_{j=1}^{n} \Gamma_{ij} \frac{dq_j}{dx}; \quad \Gamma_{ij} \equiv \frac{q_i}{f_i} \frac{\partial f_i}{\partial q_j}; \quad i, j = 1,2 \tag{9}$$

From the GCMC simulations it appears that the Ideal Adsorbed Solution Theory (IAST) of Myers and Prausnitz[22] is not completely successful in predicting the mixture loadings; see Figure 10. For this reason we estimated the component loadings, q_i, and the matrix of thermodynamic factors Γ_{ij} from the GCMC simulation data. In backing out the transport coefficients from binary mixture permeation data we note that the downstream compartment of the membrane was flushed with inert gas; for this reason we assumed the component loadings at the downstream face are negligibly small.

Figure 15 summarizes the data on the transport coefficients backed out from both unary and binary CO_2/CH_4 mixture permeation data.

.

7. References

[1] C. Baerlocher, L.B. McCusker, Database of Zeolite Structures, International Zeolite Association, http://www.iza-structure.org/databases/, 26 June 2001.

[2] E. Jaramillo, S.M. Auerbach, New force field for Na cations in faujasite-type zeolites, J. Phys. Chem. B 103 (1999) 9589-9594.

[3] S. Calero, D. Dubbeldam, R. Krishna, B. Smit, T.J.H. Vlugt, J.F.M. Denayer, J.A. Martens, T.L.M. Maesen, Understanding the role of sodium during adsorption. A force field for alkanes in sodium exchanged faujasites, J. Am. Chem. Soc. 126 (2004) 11377-11386.

[4] J.P. Ryckaert, A. Bellemans, Molecular dynamics of liquid alkanes, Faraday Discuss. Chem. Soc. 66 (1978) 95-106.

[5] D. Frenkel, B. Smit, Understanding molecular simulations: from algorithms to applications, Academic Press, 2nd Edition, San Diego, 2002.

[6] D. Dubbeldam, S. Calero, T.J.H. Vlugt, R. Krishna, T.L.M. Maesen, B. Smit, United Atom Forcefield for Alkanes in Nanoporous Materials, J. Phys. Chem. B 108 (2004) 12301-12313.

[7] J.G. Harris, K.H. Yung, Carbon Dioxide's Liquid-Vapor Coexistence Curve And Critical Properties as Predicted by a Simple Molecular Model, J. Phys. Chem. 99 (1995) 12021-12024.

[8] C.S. Murthy, K. Singer, M.L. Klein, I.R. McDonald, Pairwise additive effective potentials for nitrogen, Mol. Phys. 41 (1980) 1387-1399.

[9] K. Makrodimitris, G.K. Papadopoulos, D.N. Theodorou, Prediction of permeation properties of CO_2 and N_2 through silicalite via molecular simulations, J. Phys. Chem. B 105 (2001) 777-788.

[10] A.G. Bezus, A.V. Kiselev, A.A. Lopatkin, P.Q. Du, Molecular statistical calculation of the thermodynamic adsorption characteristics of zeolites using the atom-atom approximation. Part 1. Adsorption of methane by zeolite sodium-X, J.Chem.Soc., Faraday Trans. II 74 (1978) 367-379.

[11] A.V. Kiselev, A.A. Lopatkin, A.A. Shul'ga, Molecular statistical calculation of gas adsorption by silicalite, Zeolites 5 (1985) 261-267.

[12] A.I. Skoulidas, D.S. Sholl, Transport diffusivities of CH_4, CF_4, He, Ne, Ar, Xe, and SF_6 in silicalite from atomistic simulations, J. Phys. Chem. B 106 (2002) 5058-5067.

[13] A.V.A. Kumar, H. Jobic, S.K. Bhatia, Quantum effects on adsorption and diffusion of hydrogen and deuterium in microporous materials, J. Phys. Chem. B 110 (2006) 16666-16671.

[14] M. Gallo, T.M. Nenoff, M.C. Mitchell, Selectivities for binary mixtures of hydrogen/methane and hydrogen/carbon dioxide in silicalite and ETS-10 by Grand Canonical Monte Carlo techniques, Fluid Phase Equilib. 247 (2006) 135-142.

[15] C. Mellot, J. Lignieres, Monte Carlo SImulations of N_2 and O_2 adsorption in silicalites and CaLSX zeolites, Mol. Simulation 18 (1997) 349-365.

[16] T.J.H. Vlugt, R. Krishna, B. Smit, Molecular simulations of adsorption isotherms for linear and branched alkanes and their mixtures in silicalite, J. Phys. Chem. B 103 (1999) 1102-1118.

[17] T.J.H. Vlugt, BIGMAC, University of Amsterdam, http://molsim.chem.uva.nl/bigmac/, 1 November 2000.

[18] E. García-Pérez, J.B. Parra, C.O. Ania, A. García-Sánchez, J.M. Van Baten, R. Krishna, D. Dubbeldam, S. Calero, A computational study of CO_2, N_2 and CH_4 adsorption in zeolites, Adsorption (2007) Manuscript in press.

[19] W. Smith, T.R. Forester, I.T. Todorov, The DL_POLY Molecular Simulation Package, Warrington, England, http://www.cse.clrc.ac.uk/msi/software/DL_POLY/index.shtml, March 2006.

[20] S. Himeno, T. Tomita, K. Suzuki, S. Yoshida, Characterization and selectivity for methane and carbon dioxide adsorption on the all-silica DD3R zeolite, Microporous Mesoporous Mater. 98 (2007) 62-69.

[21] S. Himeno, S. Shimura, S. Sakurai, Light gas adsorption of all-silica DD3R zeolite: Computational and experimental investigation, 9th International Conference on Fundamentals of Adsorption, Giardini Naxos, Sicily, Italy, 2007.
[22] A.L. Myers, J.M. Prausnitz, Thermodynamics of mixed gas adsorption, A.I.Ch.E.J. 11 (1965) 121-130.
[23] S. Himeno, T. Komatsu, S. Fujita, T. Tomita, K. Suzuki, K. Nakayama, S. Yoshida, CO_2/CH_4 Permeation characteristics of a new type DDR zeolite membrane, Kagaku Kogaku Ronbunshu 33 (2007) 122-129.
[24] R. Krishna, J.M. van Baten, E. García-Pérez, S. Calero, Incorporating the loading dependence of the Maxwell-Stefan diffusivity in the modeling of CH_4 and CO_2 permeation across zeolite membranes, Ind. Eng. Chem. Res. 46 (2007) 2974-2986.
[25] J. van den Bergh, W. Zhu, J.C. Groen, F. Kapteijn, J.A. Moulijn, K. Yajima, K. Nakayama, T. Tomita, S. Yoshida, Natural Gas Purification with a DDR Zeolite Membrane; Permeation Modelling with Maxwell-Stefan Equations, 15th International Zeolite Conference, Beijing, China, 2007.

Table 1. Summary of force field used in GCMC and MD simulations

The interaction between adsorbates was calculated using Lennard-Jones potentials and electrostatic interactions using an Ewald summation method. For adsorbate-adsorbate interactions, Lorentz-Berthelot mixing rules were applied for σ and ε/k_B. Leonard-Jones interaction with the zeolite was only taken σ and ε/k_B and epsilon for the adsorbates and for the interaction with the adsorbates and with the zeolites. The charges are also shown for the pseudo atoms.

(pseudo-) atom	Atom-atom σ / Å	Atom-atom ε/k_B / K	Atom - O in zeolite σ / Å	Atom - O in zeolite ε/k_B / K	charge
CH_4	3.72	158.5	3.47	115	0
C (CO_2)	2.757	28.129	2.7815	50.2	0.6512
O (CO_2)	3.033	80.507	2.9195	84.93	-0.3256
N (N_2)	3.32	36.4	3.06	58.25	-0.40484
O (O_2)	3.0896	44.5	2.97	67.8	-0.112
He	2.28	10.223	2.62	51.235	0
Ar	3.42	124.07	3.17	95.61	0
Ne	2.789	35.7	2.798	56.87	0
H_2	2.782	38.7	2.713	79.914	0

The molecule geometries were fixed. The bond angle for CO_2 is 180°. For N_2 and O_2, a point charge is located in the middle between the two atoms, that is twice the magnitude of the charges on N and O, and opposite in sign, so that the total molecule charge is zero. The following table shows the bond lengths that were used:

bond	bond length / Å
N-N (N_2)	1.098
O-O (O_2)	1.2
C-O (CO_2)	1.16

The zeolite atoms are considered immobile. The following table shows the charges used for the zeolite atoms:

atom	charge
$O_{Zeolite}$	-1.025
$Si_{Zeolite}$	2.05

Table 2. Three-site Langmuir parameters for pure component isotherms in DDR. The saturation capacity, q_{sat}, has the units of mol kg^{-1}. The Langmuir parameters, b, have the units of Pa^{-1}.

Zeolite	Molecule	Temperature, T/K	Three-Site Langmuir parameters					
			b_A	$q_{sat,A}$	b_B	$q_{sat,B}$	b_C	$q_{sat,C}$
DDR	CO_2	300	6.52×10^{-6}	3	6.34×10^{-8}	1	1.88×10^{-9}	0.6
DDR	CH_4	300	3.66×10^{-6}	1.6	1.9×10^{-8}	1.6	3.56×10^{-11}	1
DDR	N_2	300	3.84×10^{-7}	1.8	1.1×10^{-8}	1.8	7.34×10^{-11}	1.8
DDR	Ar	300	3.06×10^{-7}	2.1	2.58×10^{-8}	1.3	1.11×10^{-9}	2
DDR	O_2	300	5.05×10^{-7}	1.8	4.46×10^{-8}	1.8	6.62×10^{-10}	1.8
DDR	H_2	300	3.12×10^{-8}	9	2.88×10^{-10}	7	8.13×10^{-12}	6
DDR	He	300	1.13×10^{-8}	10	6.84×10^{-10}	10	6.89×10^{-10}	7
DDR	Ne	300	2.16×10^{-8}	5	7.27×10^{-10}	5	8.18×10^{-12}	4

8. Captions for Figures

Figure 1. Comparison of GCMC simulations for pure component isotherms for CH_4 in DDR with experimental data of Van den Bergh et al.[25] and Himeno [20].

Figure 2. Comparison of GCMC simulations for pure component isotherms for CO_2 in DDR with experimental data of Van den Bergh et al.[25] and Himeno [20].

Figure 3. Comparison of GCMC simulations for pure component isotherms for N_2 in DDR with experimental data of Van den Bergh et al.[25] and Himeno et al.[21]

Figure 4. Comparison of GCMC simulations for pure component isotherms for O_2 in DDR with experimental data of Himeno et al.[21]

Figure 5. Pure component isotherm data for CO_2, CH_4, N_2, Ar, Ne, He, H_2, and O_2 in DDR at 300 K. The filled symbols are GCMC simulation results. The continuous solid lines are 3-site Langmuir fits with parameters specified in Table 2.

Figure 6. Framework structure of DDR, top and side views. The blue spheres of 3 Å diameter are taken to indicate the window region.

Figure 7. Probability density plots for CO_2/CH_4 mixtures in DDR.

Figure 8. Probability density plots for CH_4/N_2 mixtures in DDR.

Figure 9. Probability density plots for CO_2/Ar mixtures in DDR.

Figure 10. Pure component and binary adsorption data for CO_2/CH_4 binary mixture. For binary mixture adsorption, the CBMC simulation results are compared with IAST predictions using the pure component isotherm fits.

Figure 11. Pure component and binary adsorption data for CH_4/N_2 binary mixture. For binary mixture adsorption, the CBMC simulation results are compared with IAST predictions using the pure component isotherm fits.

Figure 12. Pure component and binary adsorption data for CO_2/Ar binary mixture. For binary mixture adsorption, the CBMC simulation results are compared with IAST predictions using the pure component isotherm fits.

Figure 13. Unary permeation fluxes of CO_2, CH_4, N_2, He, H_2, and O_2 across a DDR membrane at 298 K. Data of Himeno et al.[23]. The data is plotted as a function of the pressure at the upstream face of the membrane. The downstream pressure was assumed to be 50 kPa.

Figure 14. Transport coefficients, $\rho Đ_i/\delta$, of CO_2, CH_4, N_2, He, H_2, and O_2 across a DDR membrane at 298 K backed out from unary permeation data of Himeno et al.[23]. The data is plotted as a function of the loading at the upstream face of the membrane, q_{up}.

Figure 15. Experimental Flux vs upstream partial pressure data for CO_2 and CH_4, pure component permeation and mixture permeation data of Himeno et al.[23]. Also shown is the comparison of transport coefficients, $\rho Đ_i/\delta$, for DDR membrane backed out from unary permeation and binary mixtures containing CO_2/CH_4. The data is plotted as a function of the total mixture loading at the upstream face of the membrane, q_{up}.

DDR, CH4

Figure 1

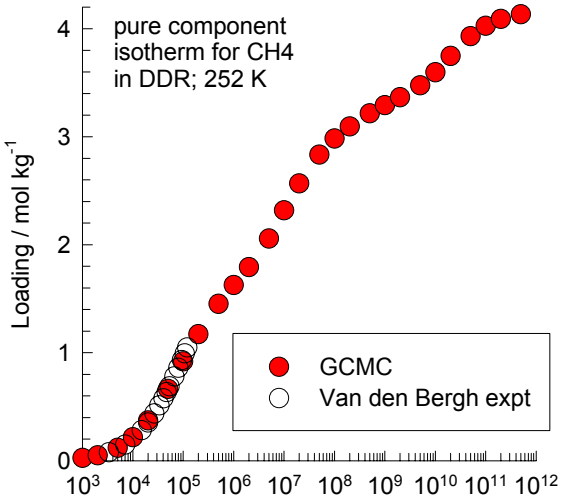

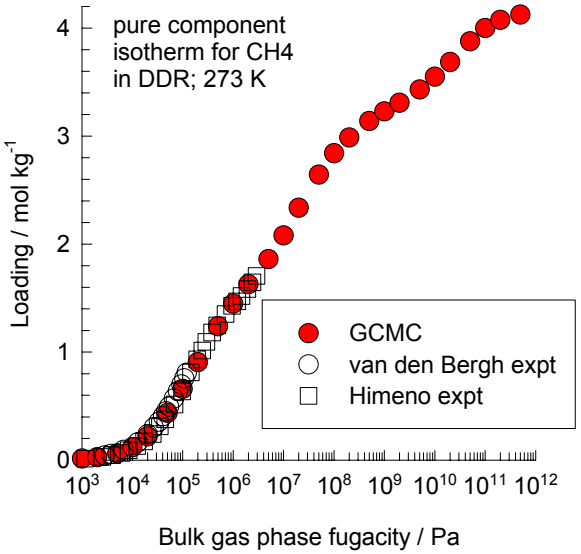

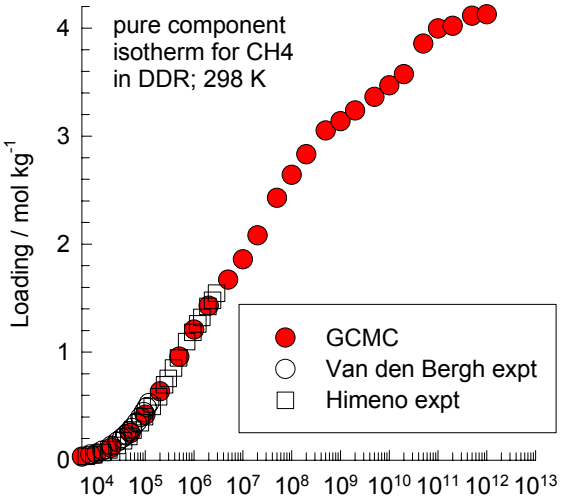

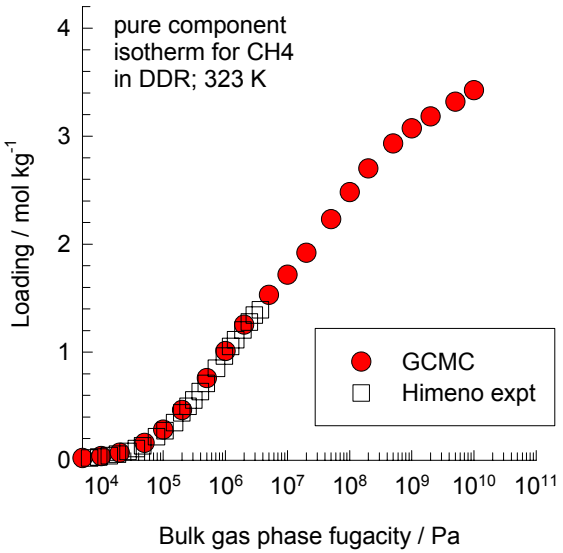

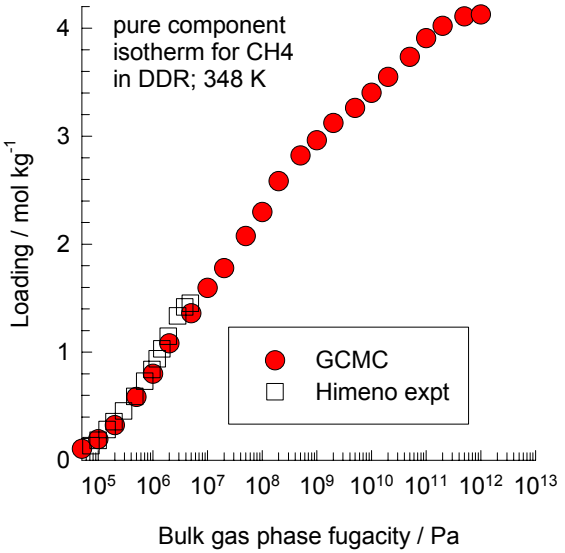

DDR, CO2

Figure 2

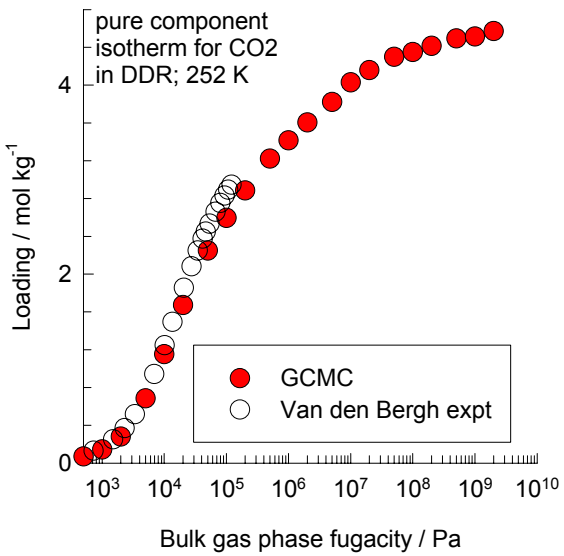

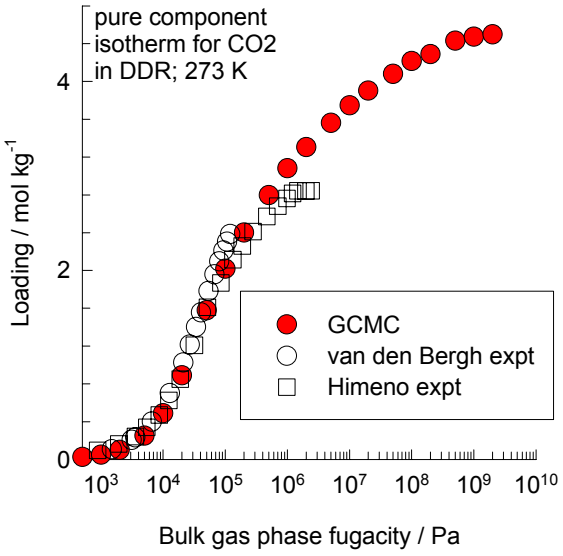

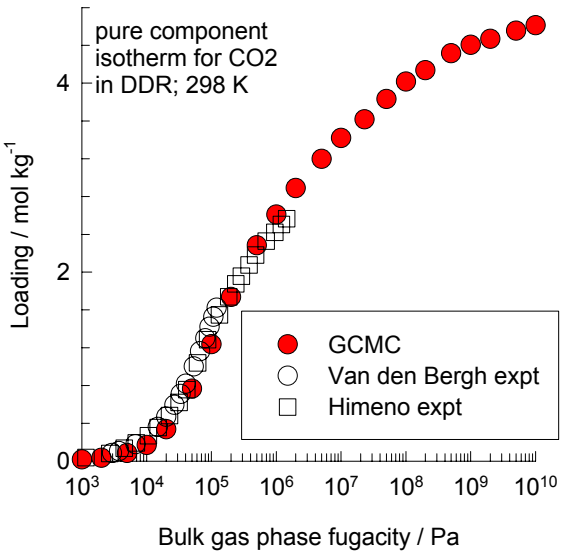

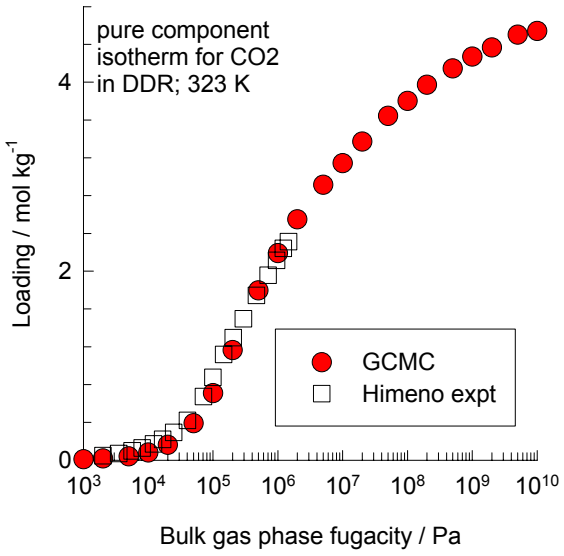

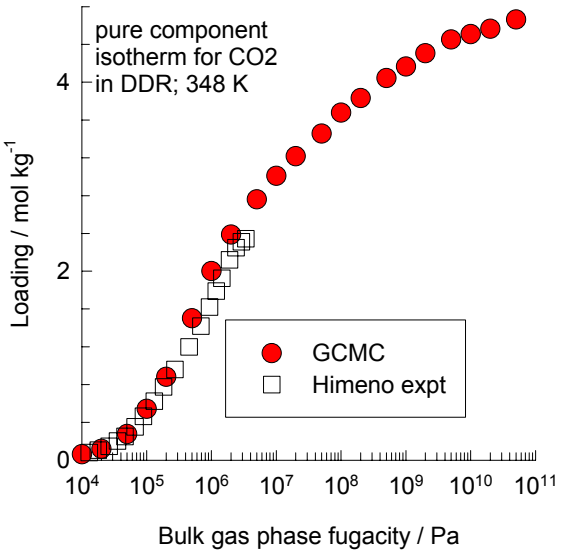

DDR, N2

Figure 3

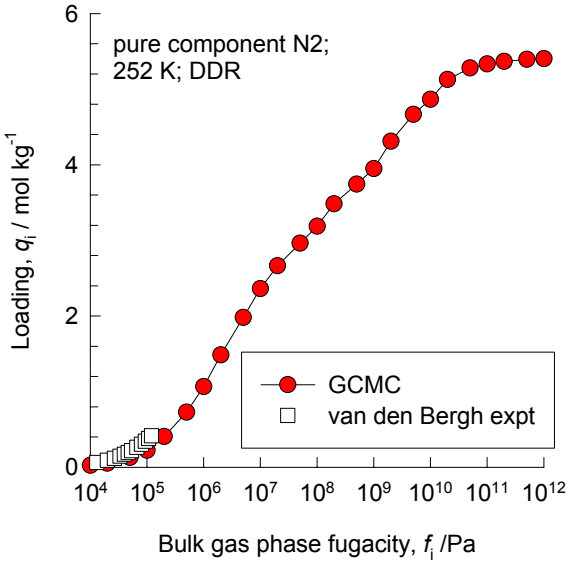

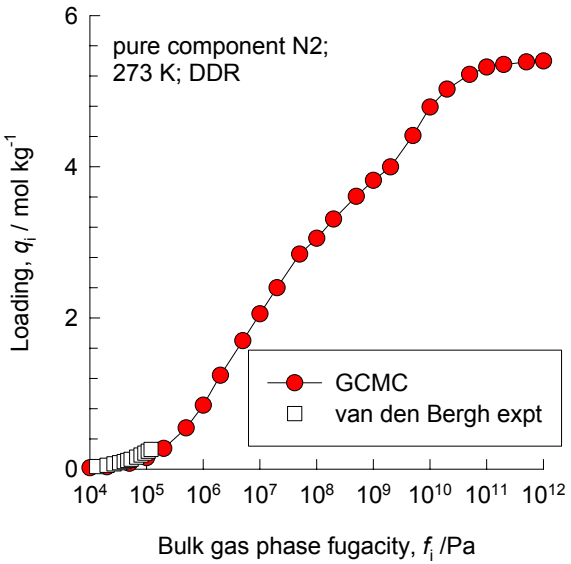

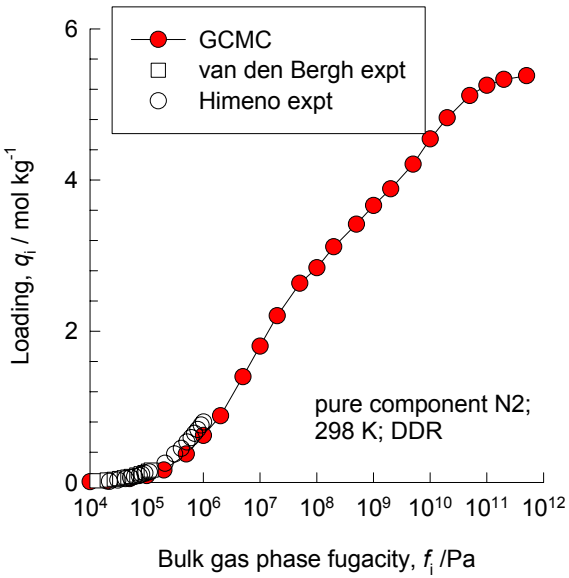

DDR, O2

Figure 4

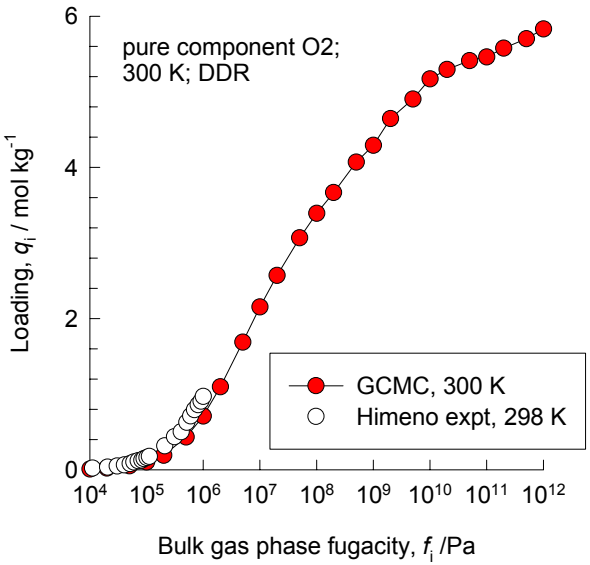

Figure 5

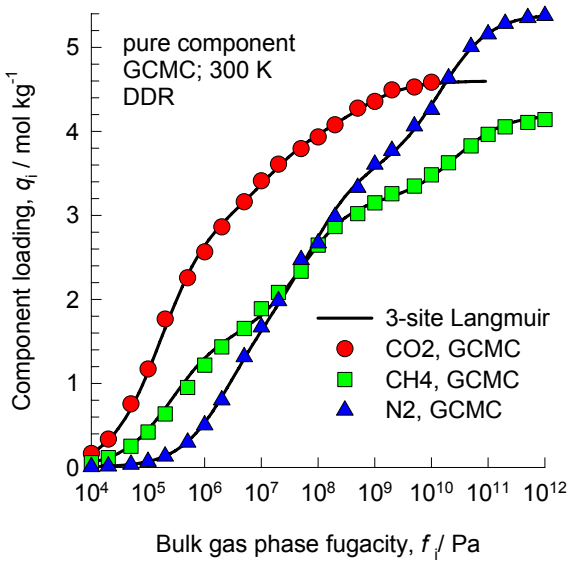
pure component
GCMC; 300 K
DDR
3-site Langmuir
CO2, GCMC
CH4, GCMC
N2, GCMC
Component loading, q_i / mol kg^{-1}
Bulk gas phase fugacity, f_i / Pa

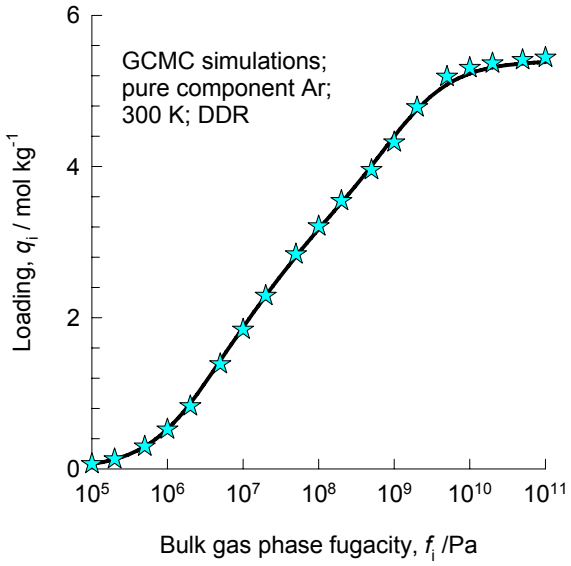
GCMC simulations;
pure component Ar;
300 K; DDR
Loading, q_i / mol kg^{-1}
Bulk gas phase fugacity, f_i /Pa

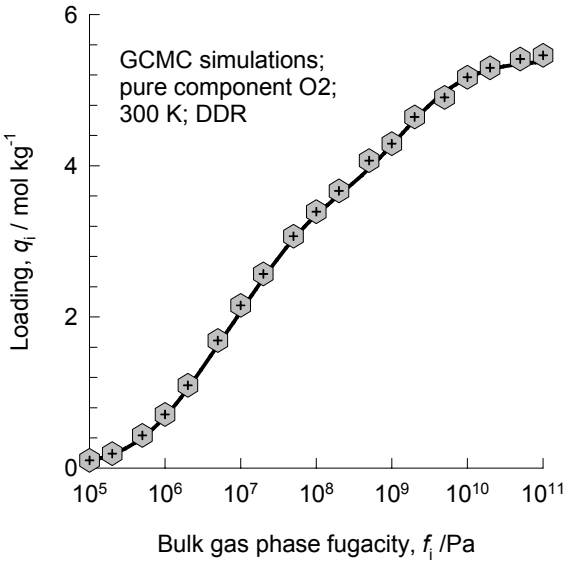
GCMC simulations;
pure component O2;
300 K; DDR
Loading, q_i / mol kg^{-1}
Bulk gas phase fugacity, f_i /Pa

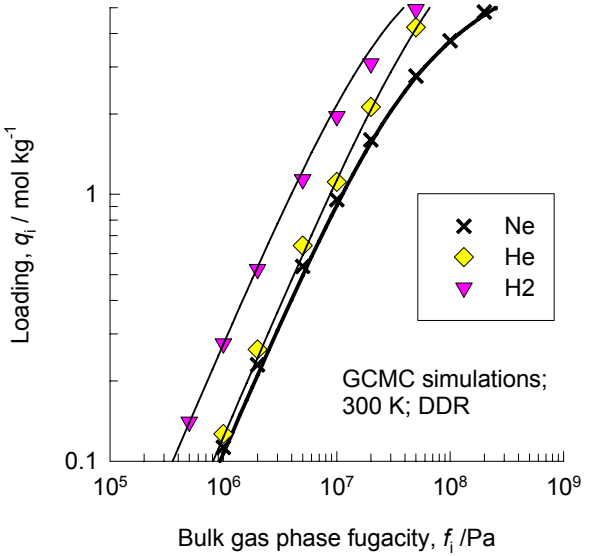
Ne
He
H2
GCMC simulations;
300 K; DDR
Loading, q_i / mol kg^{-1}
Bulk gas phase fugacity, f_i /Pa

Figure 6

Side-on view

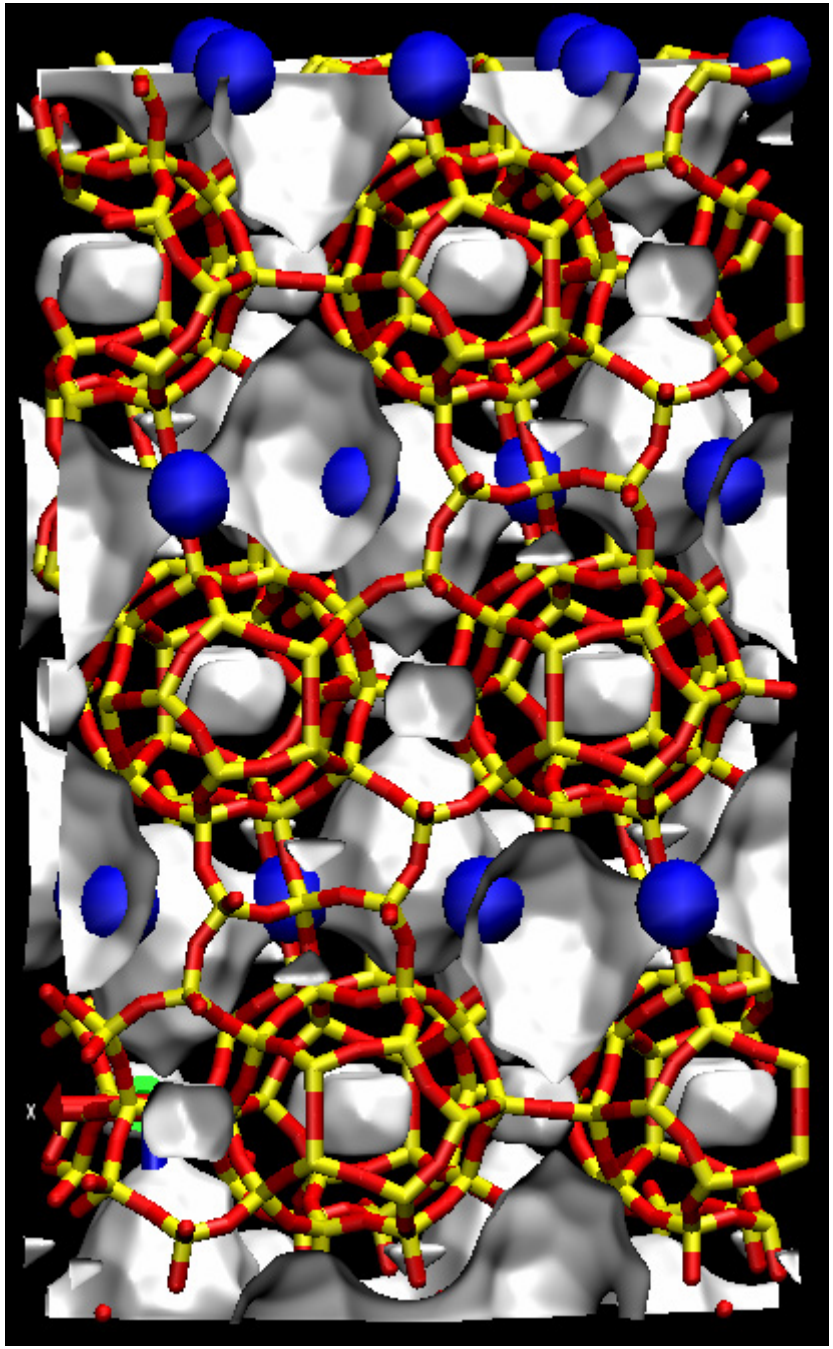

Top-down view

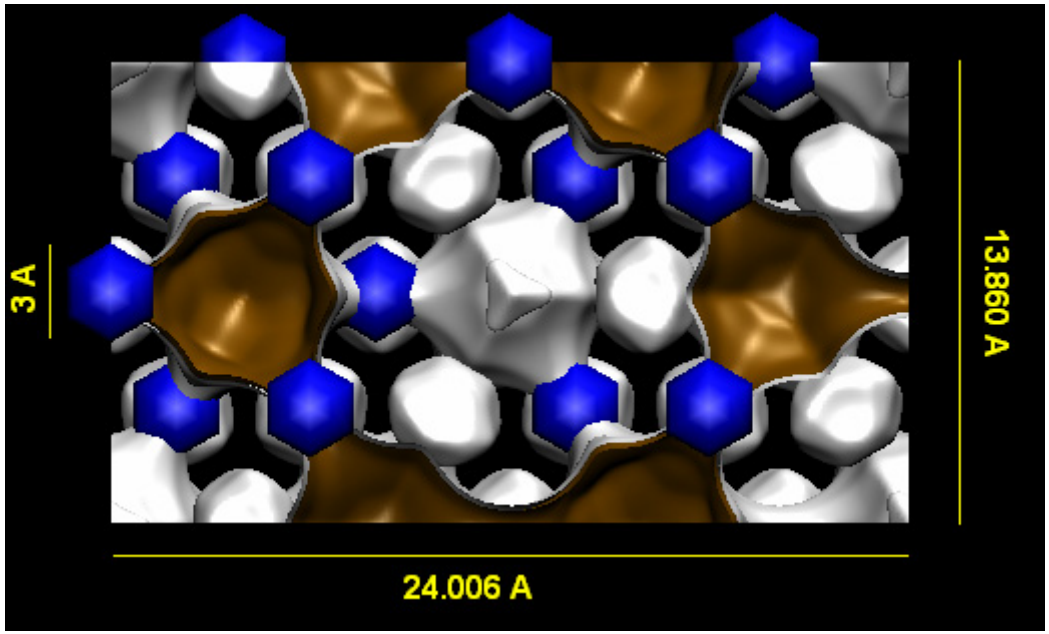

Probability density plot
of CH4-CO2 mixture in DDR
$f_1 = f_2$ =1 MPa, T = 300 K

Figure 7

Red dots = CH4
Blue dots = CO2

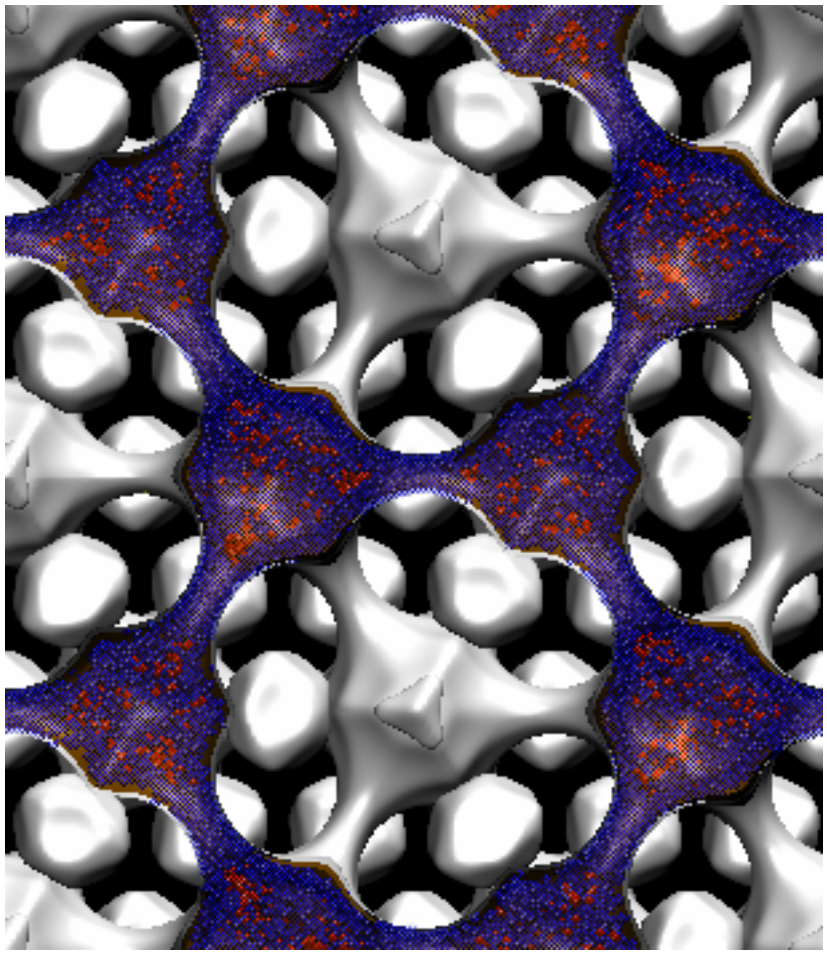

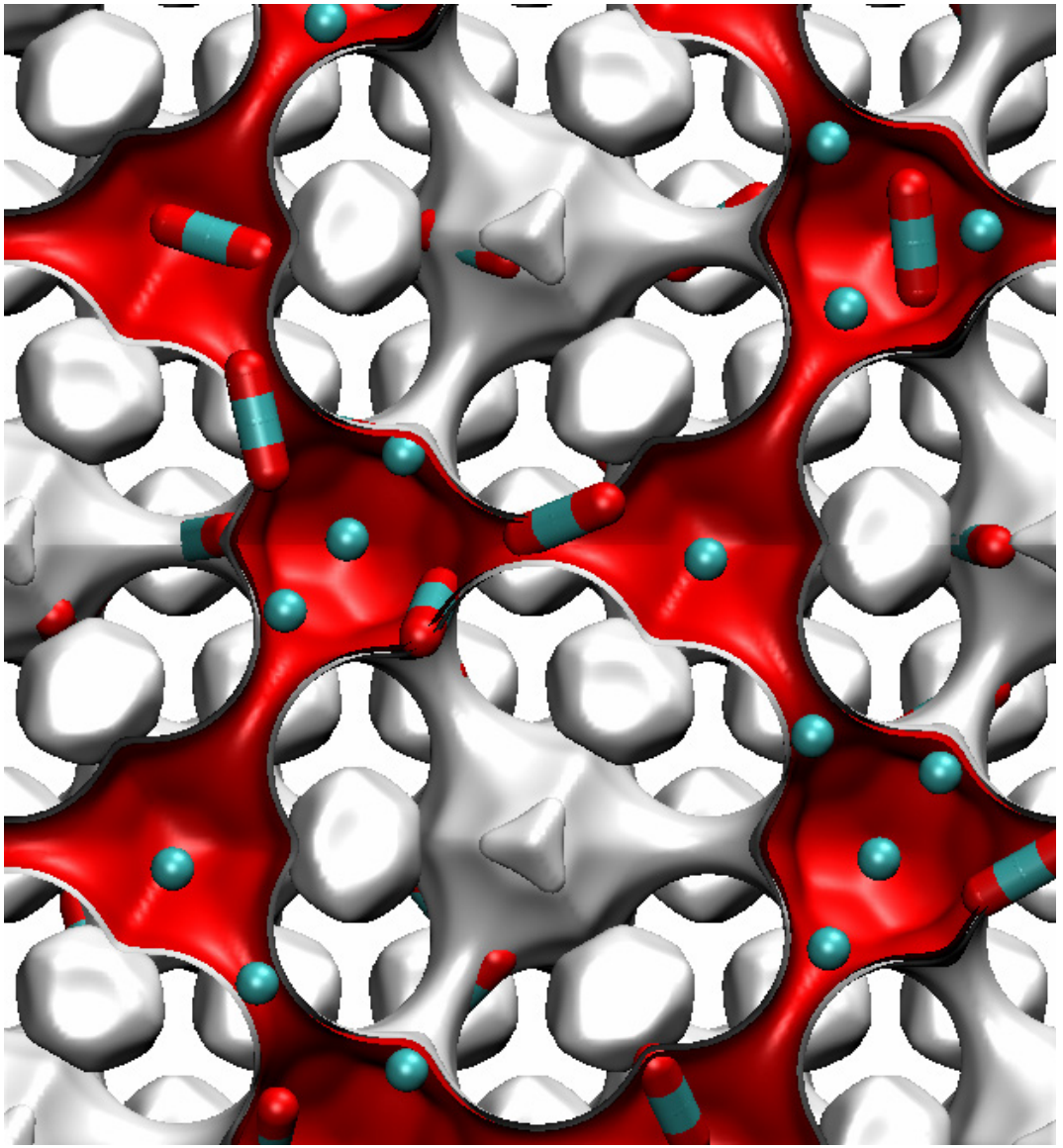

Figure 8

Probability density plot
of CH4-N2 mixture in DDR
$f_1 = f_2$ =1 MPa, T = 300 K

Red dots = CH4
Yellow dots = N2

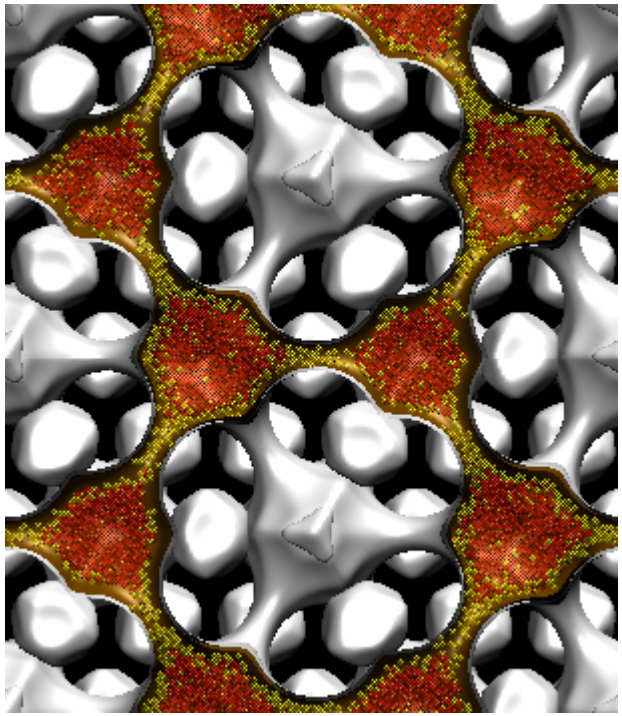

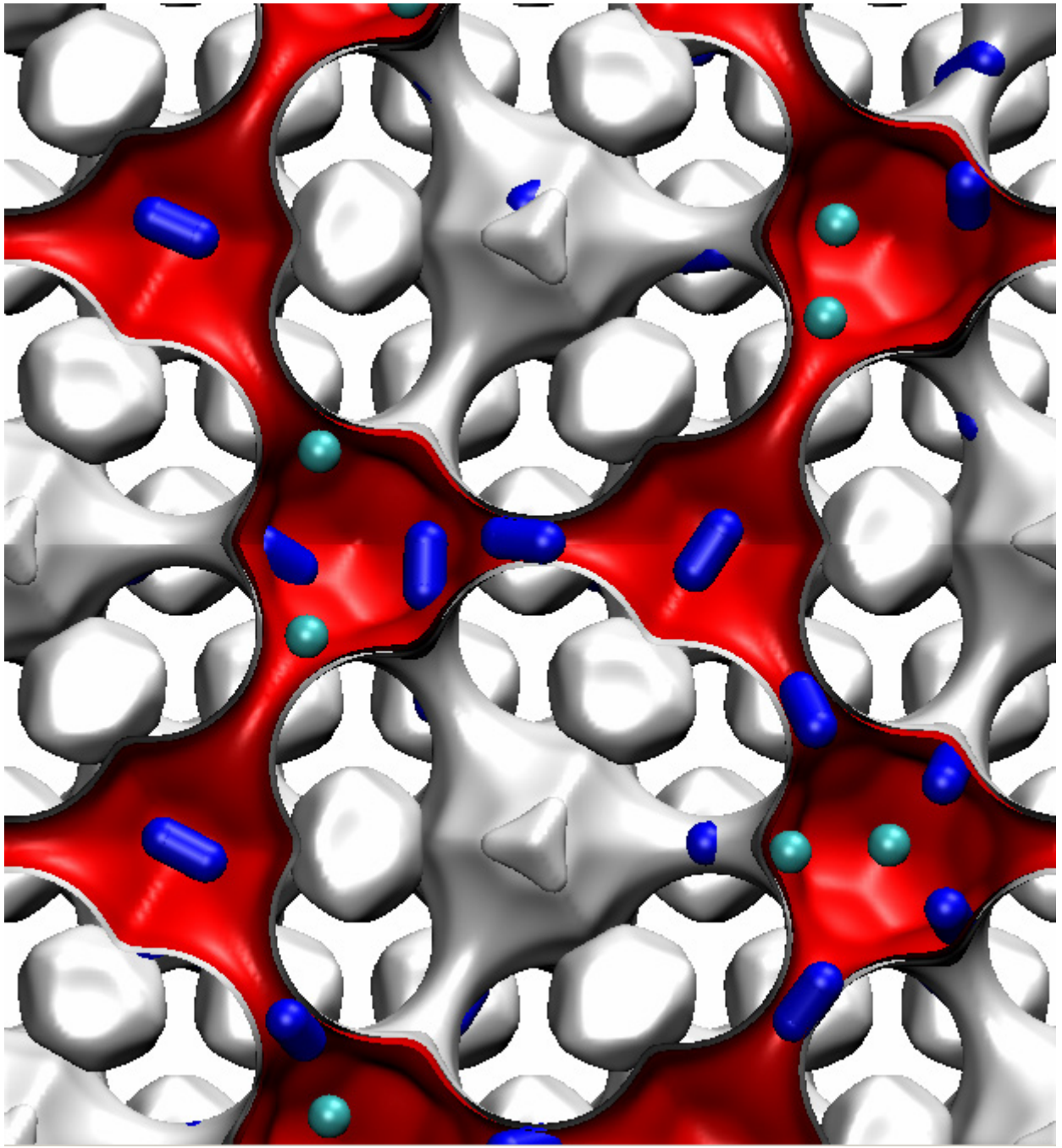

Probability density plot
of CO2-Ar mixture in DDR
$f_1 = f_2$ =1 MPa, T = 300 K

Figure 9

Blue dots = CO2
Green dots = Ar

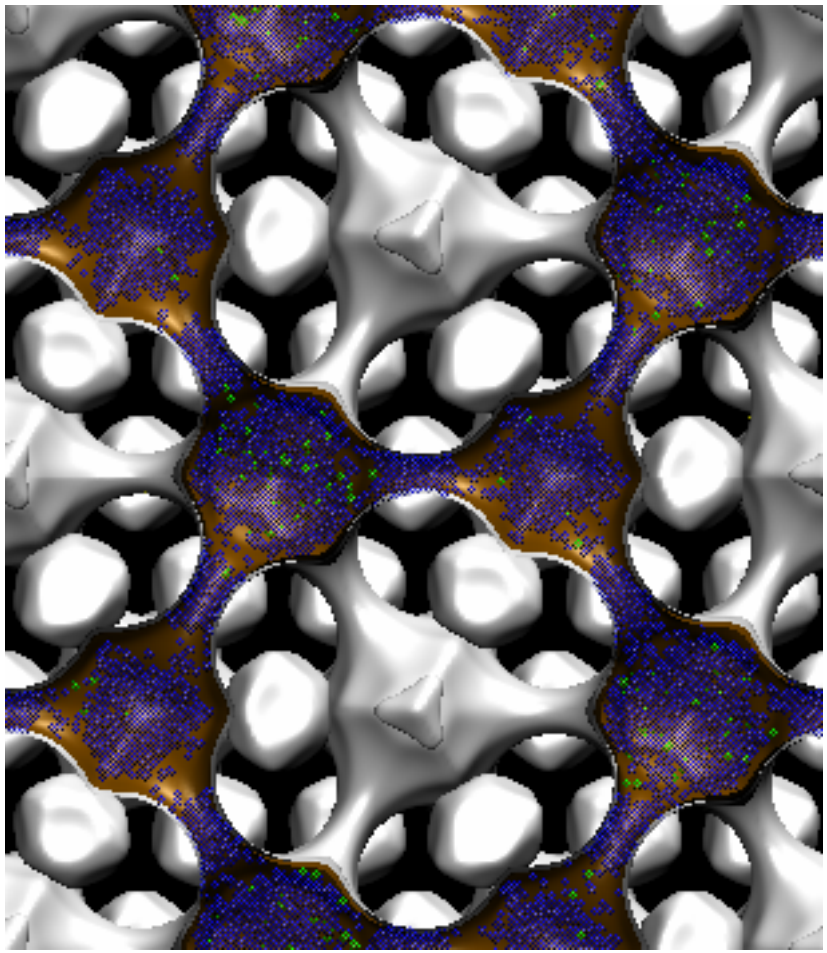

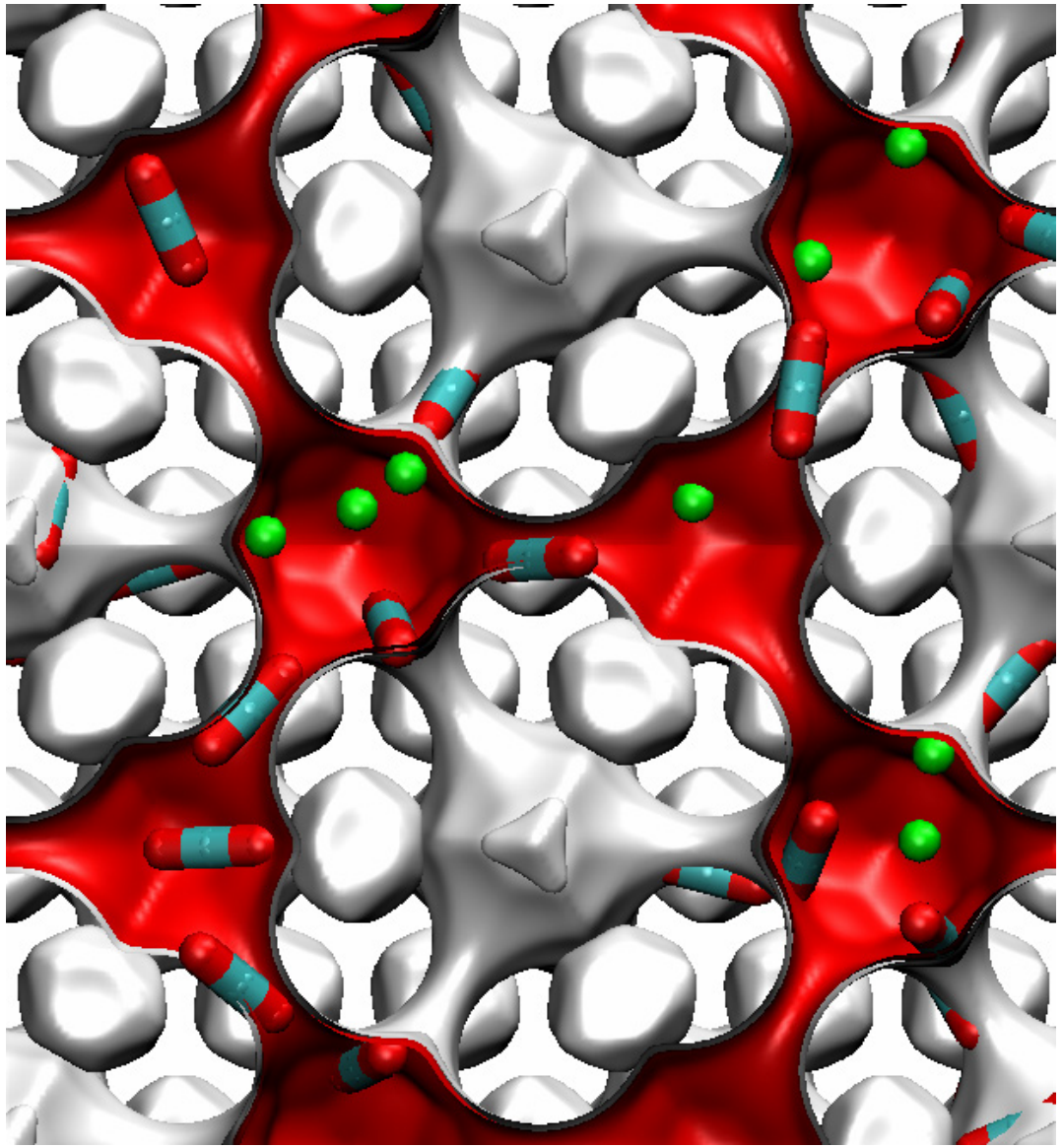

Figure 10

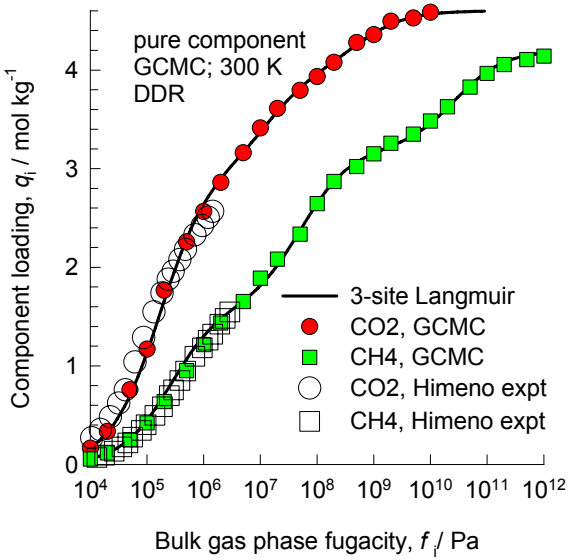

Pure components adsorption

CO2 –CH4/ DDR / 300K

mixture adsorption

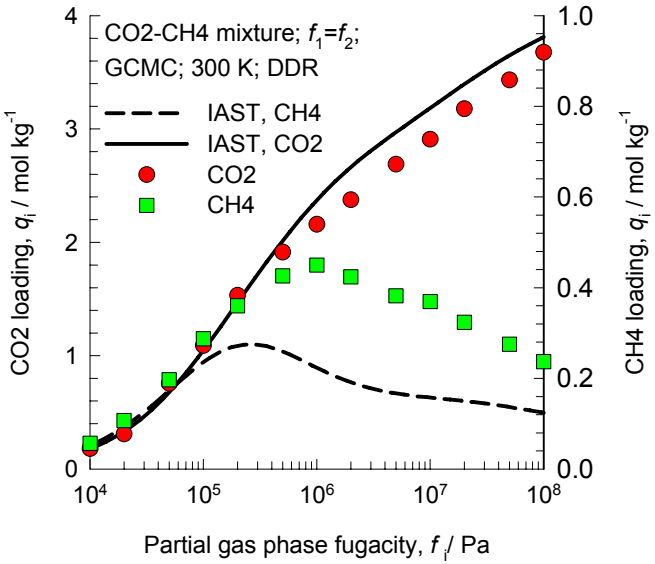

Figure 11

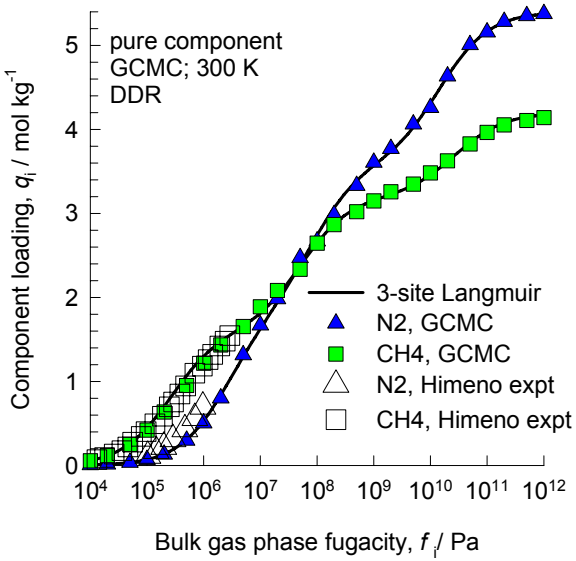

Pure components adsorption

N2 –CH4/ DDR / 300K

mixture adsorption

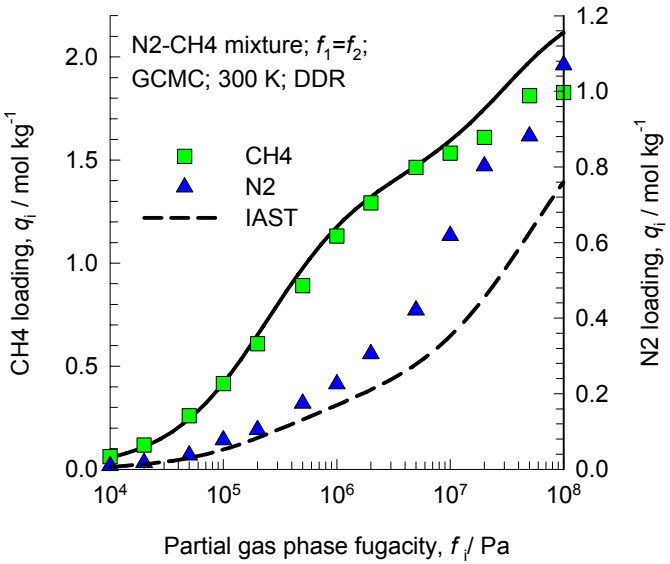

CH4-N2 mixture in DDR
T = 300 K

Figure 12

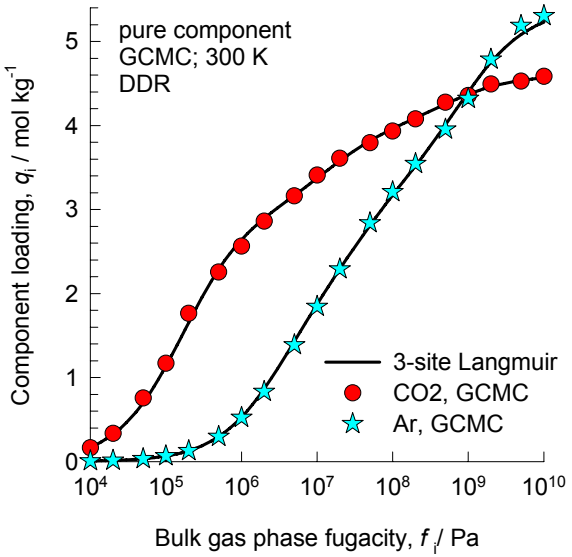

Pure components adsorption

CO2 -Ar/ DDR / 300K

mixture adsorption

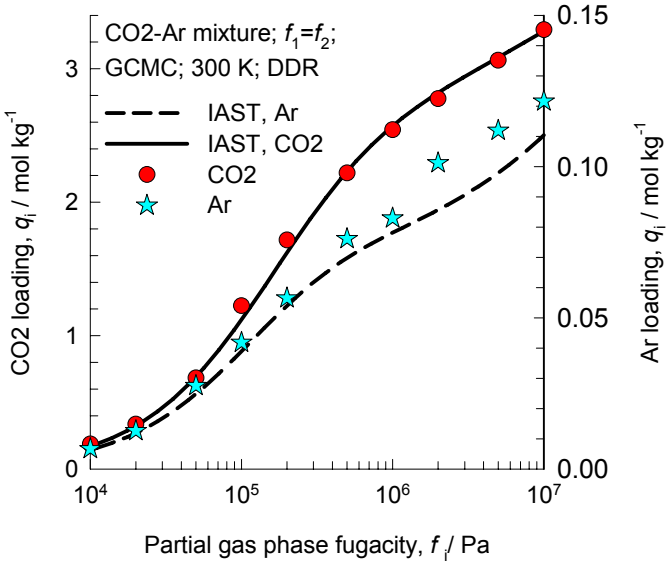

Figure 13

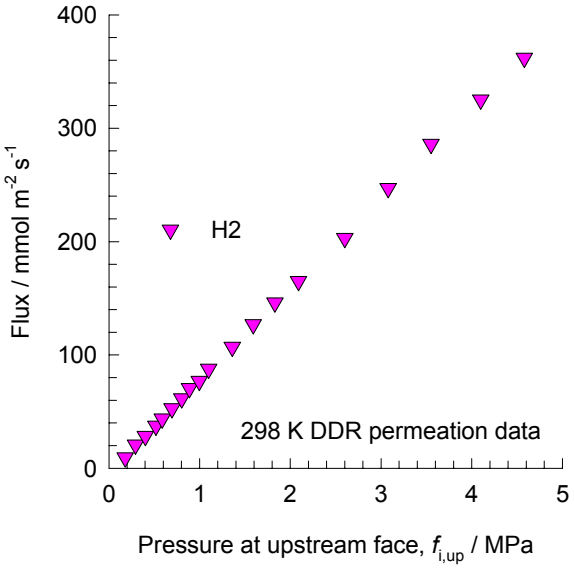
H2
298 K DDR permeation data
Flux / mmol m-2 s-1
Pressure at upstream face, fi,up / MPa

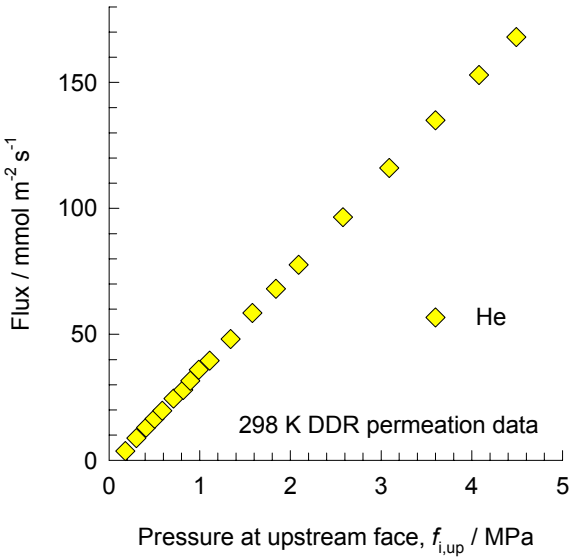
He
298 K DDR permeation data
Flux / mmol m-2 s-1
Pressure at upstream face, fi,up / MPa

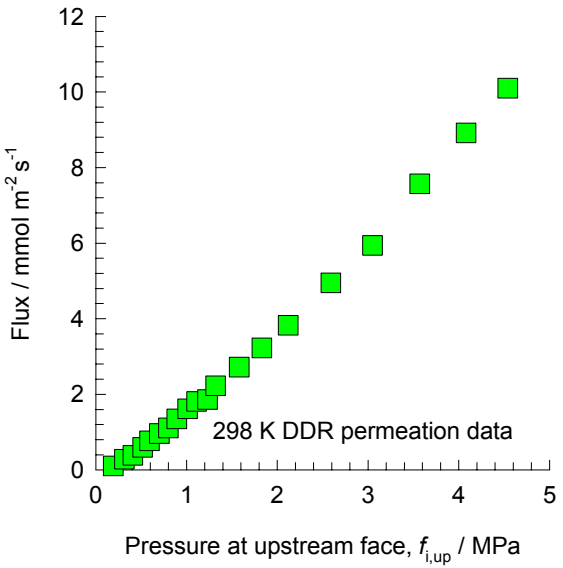
298 K DDR permeation data
Flux / mmol m-2 s-1
Pressure at upstream face, fi,up / MPa

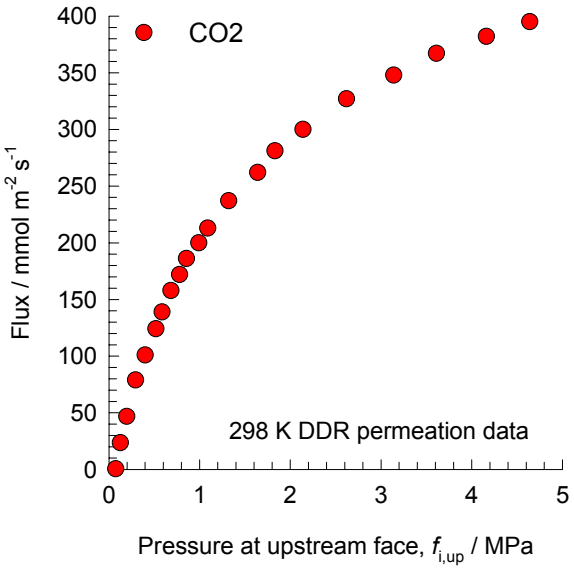
CO2
298 K DDR permeation data
Flux / mmol m-2 s-1
Pressure at upstream face, fi,up / MPa

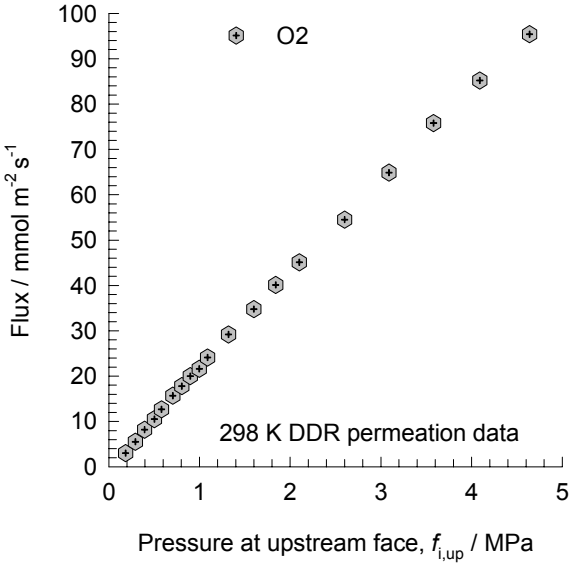
O2
298 K DDR permeation data
Flux / mmol m-2 s-1
Pressure at upstream face, fi,up / MPa

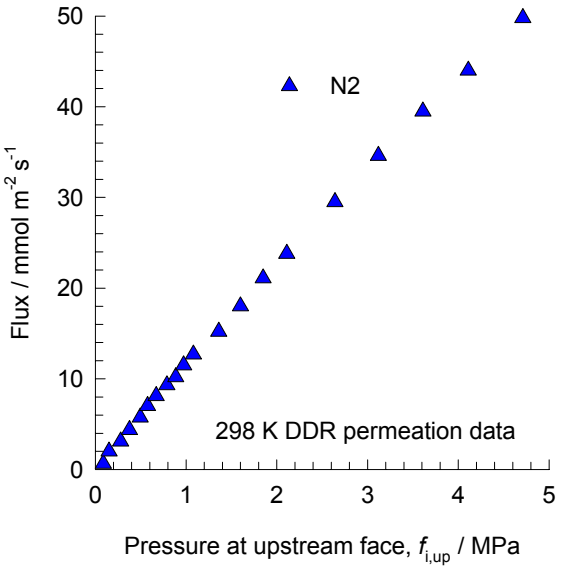
N2
298 K DDR permeation data
Flux / mmol m-2 s-1
Pressure at upstream face, fi,up / MPa

Figure 14

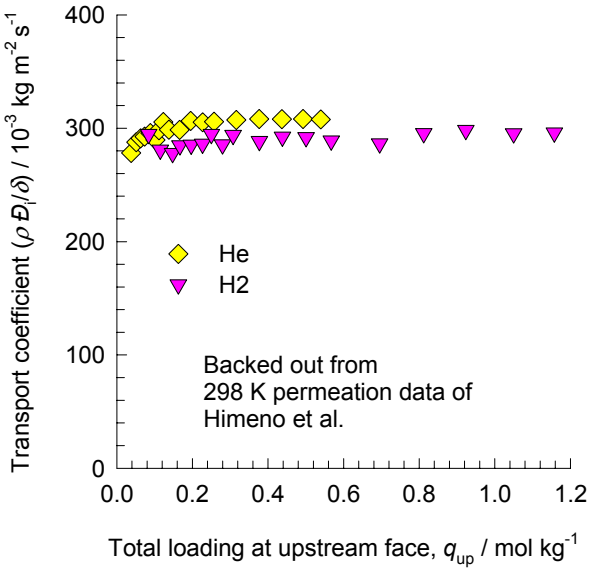
Transport coefficient ($\rho Đ_i/\delta$) / 10^{-3} kg m^{-2} s^{-1}
400
300
200
100
0
0.0
0.2
0.4
0.6
0.8
1.0
1.2
He
H2
Backed out from
298 K permeation data of
Himeno et al.
Total loading at upstream face, q_{up} / mol kg^{-1}

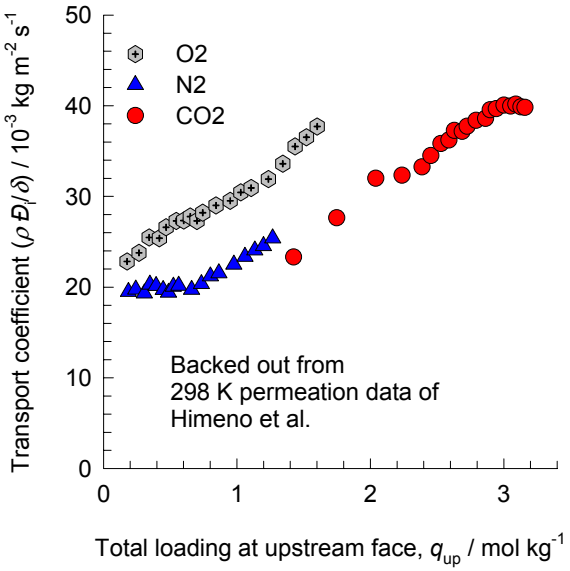
Transport coefficient ($\rho Đ_i/\delta$) / 10^{-3} kg m^{-2} s^{-1}
50
40
30
20
10
0
0
1
2
3
O2
N2
CO2
Backed out from
298 K permeation data of
Himeno et al.
Total loading at upstream face, q_{up} / mol kg^{-1}

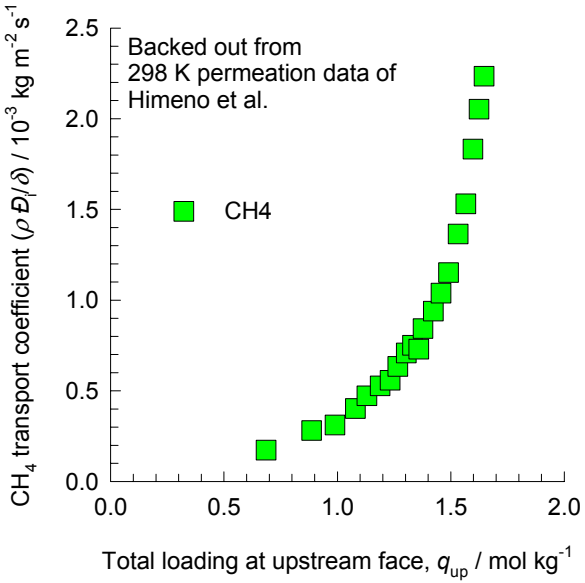
CH_4 transport coefficient ($\rho Đ_i/\delta$) / 10^{-3} kg m^{-2} s^{-1}
2.5
2.0
1.5
1.0
0.5
0.0
0.0
0.5
1.0
1.5
2.0
Backed out from
298 K permeation data of
Himeno et al.
CH4
Total loading at upstream face, q_{up} / mol kg^{-1}

Figure 15

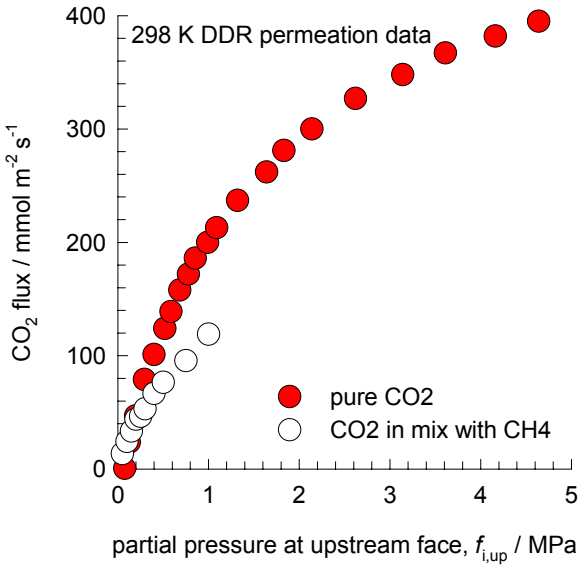
298 K DDR permeation data
pure CO2
CO2 in mix with CH4
CO2 flux / mmol m-2 s-1
partial pressure at upstream face, fi,up / MPa

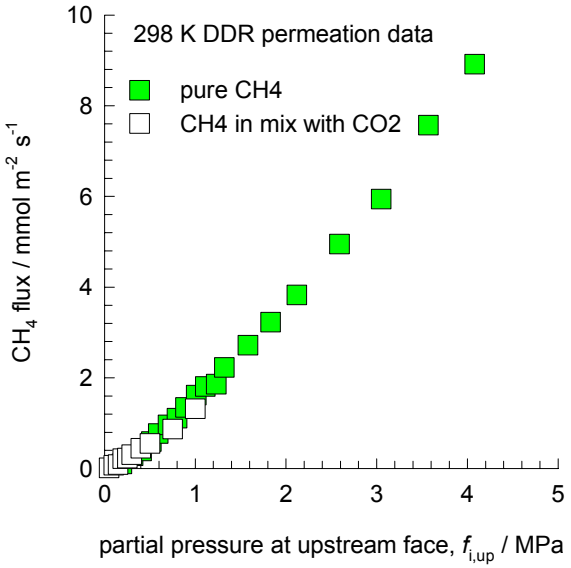
298 K DDR permeation data
pure CH4
CH4 in mix with CO2
CH4 flux / mmol m-2 s-1
partial pressure at upstream face, fi,up / MPa

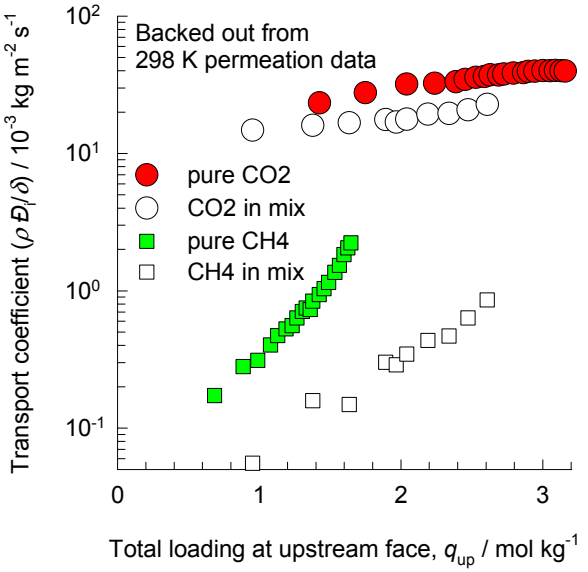
Backed out from
298 K permeation data
pure CO2
CO2 in mix
pure CH4
CH4 in mix
Transport coefficient (ρĐi/δ) / 10-3 kg m-2 s-1
Total loading at upstream face, qup / mol kg-1